揚州大學
YANGZHOU UNIVERSITY

本科生毕业论文

毕业论文题目 Quantum dot based light-emitting electrochemical cells: mechanism and recent advances

学生姓名 RAKIB ABDULLAH AL

学号 188801368

所在学院 物理科学与技术学院

专业及班级 微电 18

指导教师 刘红飞

完成日期 2022 年 5 月 3 日

Abstract

Architects, interior and automobile designers all around the world are now inspired by large-area, ultrathin light-emitting devices. The most potential next-generation device designs for future flexible and large-area lighting technologies are light-emitting electrochemical cells (LECs) and quantum dot light-emitting diodes (QD-LEDs). Both approaches use solution-based manufacturing processes, making them appealing for low-cost applications based on roll-to-roll fabrication or inkjet printing, for example. Both approaches, however, offer distinct advantages that explain their attraction.

Due to their remarkable optical qualities, color purity with a restricted emission range, and solution processability, quantum dots (QDs) have secured their place in lighting applications. They've recently been used in light-emitting electrochemical cells (LECs). Based on solution manufacturing processes and air-stable electrode materials, this technology provides a potential large-area device idea. With maximum brightness up to 1000 cd/m2 and current efficiency of 1.9 cd/A, LECs based on CdSe/CdS core/shell QDs provide brilliant, uniform, and extremely voltage-independent electroluminescence, equivalent to multilayer QD-based light-emitting diodes (LEDs). The drop-in photoluminescence quantum yield (/) following the ligand-exchange process, as well as the unstable blue emission, are two limits that must be overcome. These unwanted properties are not present in newly developed hybrid organic–inorganic or entirely inorganic perovskite nanocrystals (NCs). They have high / no surface passivation, configurable band gaps by quantum confinement or simple modifications in composition, and no spectrum widening from high surface trap densities, unlike core/shell QDs. All of these properties make perovskite QDs a strong contender for use as the emitting material in LECs.

KEYWORDS: Light-Emitting Electrochemical Cells (LECs), LECs mechanism, Quantum Dots (QDs), Colloidal quantum dots, Core/shell quantum dots, Perovskite Nanocrystals,

Table of Contents

1. Introduction 4
2. Light-emitting electrochemical cells (LECs)? 5
2.1 What is Light-emitting electrochemical cells (LECs)? 5
2.2 Operation mechanism of Light-emitting electrochemical cells (LECs) ....**Error! Bookmark not defined.**
3. Introduction of Quantum Dots (QDs) 10
4. Quantum Dots (QDs) in Light-emitting electrochemical cells (LECs) 11
4.1 Introduction to Semiconductor Nanocrystals 11
4.2 Colloidal QDs 12
4.3 Type -I Core-Shell NCs 13
4.4 CdSe-Based QDs—QDs Used in LECs 14
4.5 Perovskites 15
4.6 Perovskite Nanostructures 17
4.7 Synthesis of Perovskite NCs 18
5. Applications of NCs into LECs 21
5.1 Core-Shell QDs Emitters for LECs 21
5.2 Perovskite Emitters for LECs 25
6. Conclusion 28
Acknowledgments 29
References 30

1. Introduction

Future lighting goods and applications will go far beyond the mere generation of light, as large-area and flexible lighting technologies, as well as the related creative design options, become increasingly inspiring. Prototypes of light-emitting wallpapers, windows, stickers, and dynamic rear lights, for example, are being developed. The next generation of lighting technologies will be able to surpass the limitations of epitaxial LEDs in terms of form ability and flexibility, allowing light sources to be installed in goods with less space. Furthermore, large-area solution-based and cost-effective manufacturing processes will pave the way for new application fields and market segments, such as disposable electronics and smart fabrics, to emerge.

Aside from the well-studied organic light-emitting diodes, light-emitting electrochemical cells (LECs) are a viable option for large-area device designs (OLEDs). The integration of ionic species into the active light-emitting layer is the fundamental distinction from OLEDs. In its most basic form, the LEC device consists of a single active layer sandwiched between two electrodes and made up of a combination of active material and ionic species.

Architects, interior and automobile designers all around the world are now inspired by large-area, ultrathin light-emitting devices. The most potential next-generation device designs for future flexible and large-area lighting technologies are light-emitting electrochemical cells (LECs) and quantum dot light-emitting diodes (QD-LEDs). Both approaches use solution-based manufacturing processes, making them appealing for low-cost applications based on roll-to-roll fabrication or inkjet printing, for example. Both approaches, however, offer distinct advantages that explain their attraction. LECs use ionic species in the active layer, which eliminates the need for extra organic charge injection and transport layers, as well as reactive cathode materials, making them stand out for their simplicity. Colloidal quantum dots (QDs) are semiconducting nanocrystals that demonstrate high yield light emission, which can be readily controlled throughout the whole visible spectrum by material composition and size. QD-LEDs impress with their purity and profusion of accessible hues. Emerging technologies that combine the potential of both concepts (LEC and QD-LED) are discussed, either by extending a typical LEC architecture with additional QDs or by replacing the entire organic LEC emitter with QDs or perovskite nanocrystals while maintaining the simple LEC setup characterized by the incorporation of mobile ions.

2. Light-Emitting Electrochemical Cell (LECs)

2.1 What is Light-emitting Electrochemical Cell (LECs)?

The light-emitting electrochemical cells (LECs) is a type of organic optoelectronic device that uses electron–hole recombination in an organic semiconductor to generate light from energy. The inclusion of mobile ions in the active layer is a key feature of LECs, which results in complex device physics and, more crucially, efficient and reliable functioning in a simple device setup.

The light-emitting electrochemical cell (LEC) is a layered planar device that, in its most basic form, consists of an electroluminescent organic semiconductor (OSC) as the active material sandwiched between an anode and a cathode, as shown schematically in Fig. 1a. It is usual practice to construct the constituent active-material and electrode layers on a substrate to offer mechanical robustness to the device because they can be quite thin, with a typical thickness of *100 nm. Furthermore, because the light is generated within the active material, one of the electrodes (and the substrate if the bottom electrode is transparent) must be transparent, whilst the other electrode is typically reflective to direct all of the light exiting the device forward.

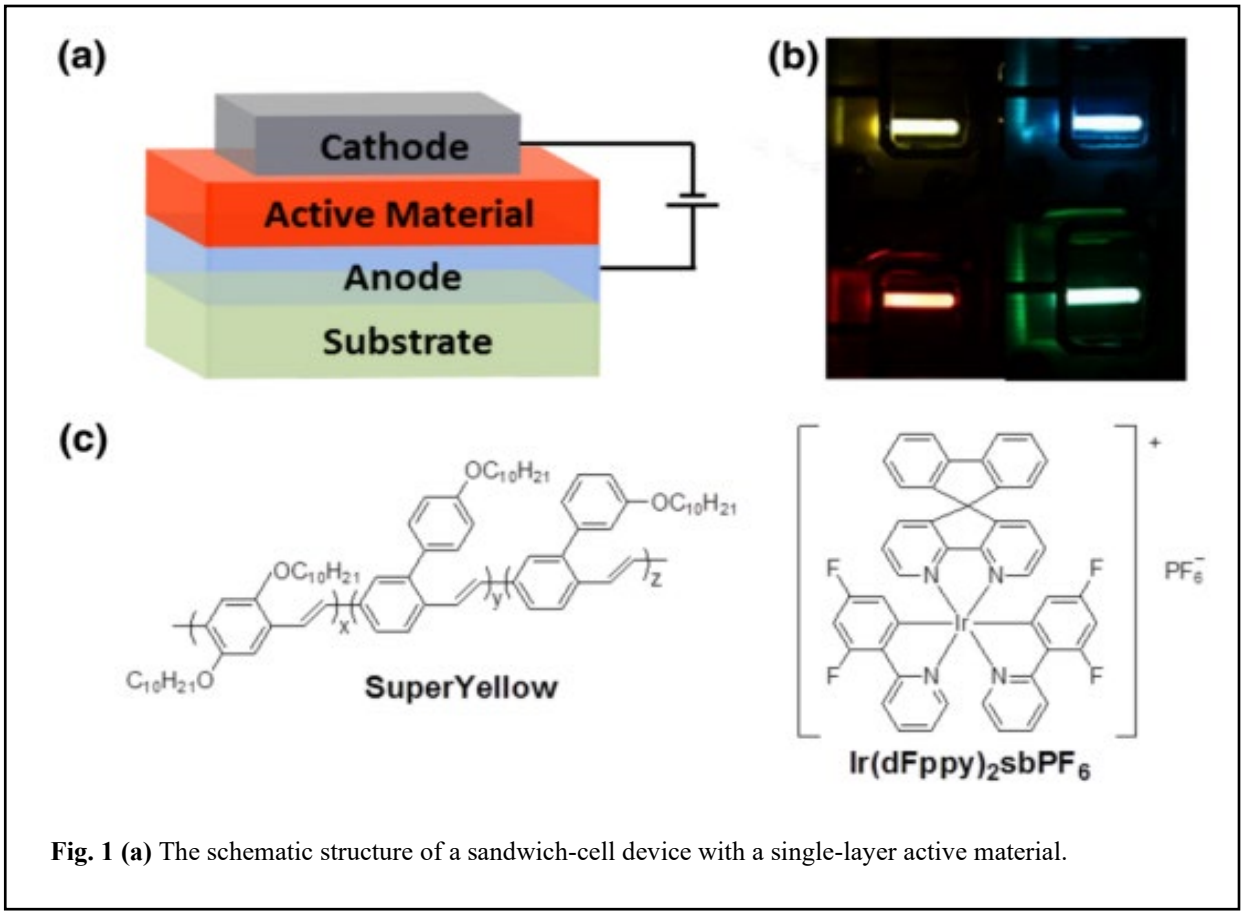

Fig. 1 (a) The schematic structure of a sandwich-cell device with a single-layer active material.

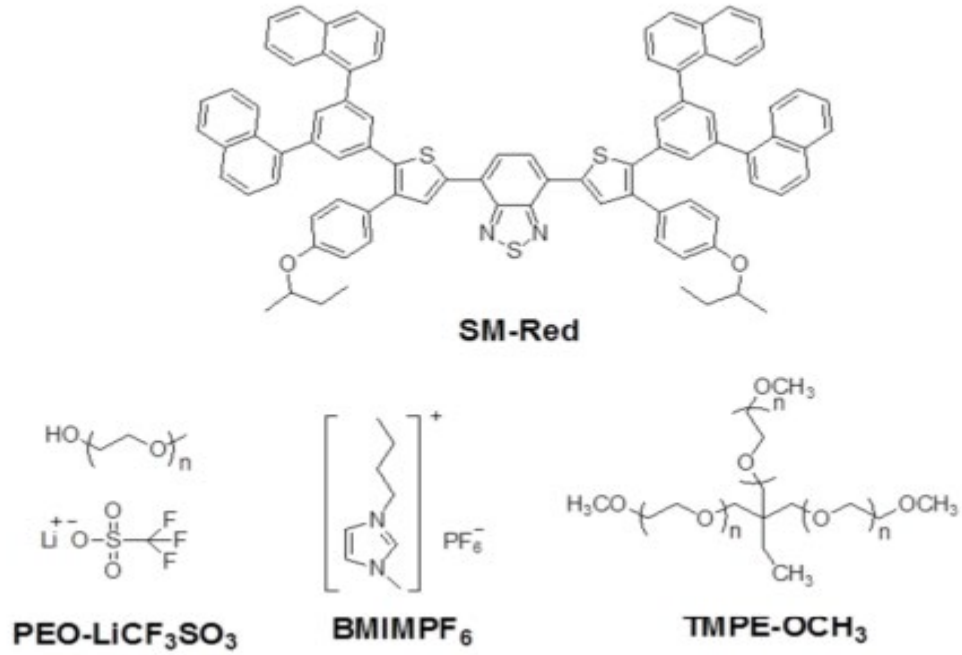

Fig. 1 (b) A photograph of the light-emission from four LEC devices based on organic semiconductors with different energy gaps, as manifested in the corresponding variety in the emission color. (c-Top) The chemical structures of three emitting compounds: the conjugated polymer Super Yellow, the ionic transition metal complex Ir(dFppy)2sbPF6, and the small molecule SM-Red. (c-Bottom) The chemical structure of three electrolyte constituents: the solid polymer electrolyte PEO: LiCF3SO3, the ionic liquid BMIMPF6, and the ionic transporter TMPE-OCH3.

The ions in the active material redistribute in an intricate manner to facilitate efficient injection, transport, and recombination of electrons and holes when a sufficient voltage is applied between the two electrodes (larger than the energy gap of the OSC, commonly V = 3–5 V); and after a turn-on time, light is emitted from the active material and coupled out of the device through the transparent electrode. Sect. 2 describes the turn-on procedure in full. As a result, the LEC emits low voltage area emission with a hue determined by the OSC's energy gap. Because the energy gap is determined by the chemical structure, and because OSCs have such a wide structural variability, an LEC can produce almost any emission color. Figure 1b shows a photo of four operational LECs made up of OSCs with varying energy gaps and a wide variety of emission colors ranging from red to blue.

Pei and collaborators are credited with developing the LEC, which utilized a conjugated polymer (CP) as the OSC and a solid polymer electrolyte as the source of mobile ions in their groundbreaking 1995 paper [1, 2]. Soon after, Lee and colleagues demonstrated that functional LEC devices could be made with a single-component active material that included an ionic transition metal complex (iTMC) that acted as both the OSC and a source of mobile anions [3]. However, it should be noted that, in order to achieve a reasonable turn-on time, the vast bulk of

subsequent research on iTMC-LECs has used an extra electrolyte (typically an ionic liquid) [4, 5]. Although new groups of functional materials, including as non-ionic luminous small molecules [6–14], ionic fluorescent small molecules [15–17], quantum dots [18, 19], and perovskites [20, 21], have appeared more recently, the LEC field has been dominated by these two primary classes of chemicals. The chemical structures of a CP, an iTMC, and a luminous small molecule, as well as a number of electrolytes used in contemporary high-performance LEC devices, are shown in Figure 1c.

Early on, it was recognized that functional LEC devices may use air stable materials for both electrodes and that the active material might come in a variety of thicknesses. This material tolerance opened the door to unprecedented "easy" solution-based manufacturing of emissive devices, with one particularly appealing potential being high-speed roll-to-roll manufacture of flexible LEC sheets, similar to how newspapers and magazines are made. This area of LEC research and development has finally taken off in recent years, and Sect. 3 highlights recent achievements in LEC fabrication that are both cost-effective and scalable.

Despite this intriguing potential, total LEC research and development activity has been quite minimal. This can be explained by the fact that LEC devices have consistently underperformed another area-emissive device based on an OSC: the organic light-emitting diode (OLED). In this perspective, the fact that LEC device performance has increased considerably in recent years is encouraging. We present developments in Sect. 4 that have enabled this improvement, such as fine-tuning the active material's composition, designing and synthesizing materials with improved chemical and electrochemical stability, and implementing appropriate drive-current protocols; we quantify how the LEC efficiency has improved. Before moving on to more particular current developments in the LEC field, we'd like to acknowledge and draw the reader's attention to earlier essential summaries and reviews on LEC research, as provided by Refs. [22–34].

2.2 Operation mechanism of Light-emitting electrochemical cells (LECs)

Since their discovery by Pei et al. [35–37], the functional principle of LECs has been the topic of heated controversy. The electrodynamic model (ED) [38–41] and the electrochemical doping model (ECD) [42–47] have both been developed, and measurement data have been interpreted using either of them. However, in recent years, a mechanistic consensus has emerged, and both models have been shown to be fairly limiting examples of a unifying description (Fig. 2) [48]. The present knowledge of the functional principle of LECs is briefly addressed in the next section.

The initial step in LEC functioning is to redistribute the ions in the active layer after applying an external bias. Anions and cations migrate to the electrode interfaces, driven by the electrical field, to create thin sheets of uncompensated charge known as electric double layers (EDLs)[48–51]. The thickness of these EDLs was reported to be in the range of 2–6 nm for pLECs in sandwich form using impedance spectroscopy [49,51]. At low biases, typically below 2.5 V,

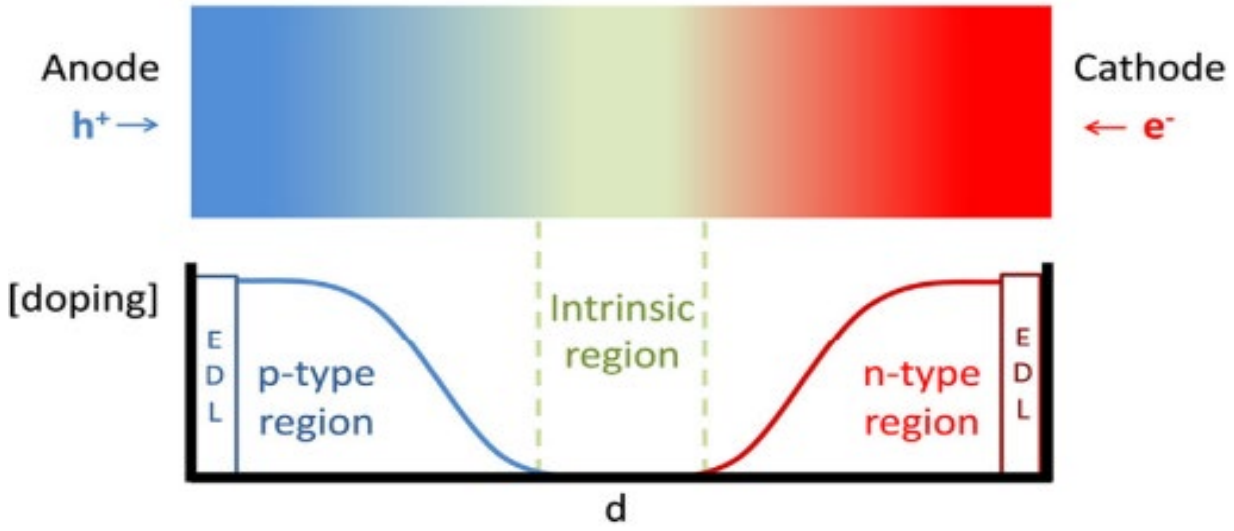

Fig 2: Schematic representation of the operation mechanism of LECs at sufficient high voltages after formation of the electric double layers (EDLs) and the p- and n-type doped zones.

carrier injection is limited, and ionic transport and electronic charge carrier diffusion dominate the device current. The entire applied potential decreases over the EDLs in this case, leaving the majority of the active layer field-free [48].

The initial step in LEC functioning is to redistribute the ions in the active layer after applying an external bias. Anions and cations migrate to the electrode interfaces, driven by the electrical field, to create thin sheets of uncompensated charge known as electric double layers (EDLs)[48–51]. The thickness of these EDLs was reported to be in the range of 2–6 nm for pLECs in sandwich form using impedance spectroscopy [49,51]. At low biases, typically below 2.5 V, carrier injection is limited, and ionic transport and electronic charge carrier diffusion dominate the device current. The entire applied potential decreases over the EDLs in this case, leaving the majority of the active layer field-free [48].

However, the device emits a relatively low brightness in these conditions. Only at higher biases, often greater than 2.5 V, do brightness levels reach application-relevant levels. At such biases, substantially more charges are injected, causing the semiconducting material to oxidize and reduce. The uncompensated ions of opposite sign present at the electrode interfaces stabilize these oxidized and reduced species, which are identical to those generated by chemical oxidation and reduction in doped organic devices [51]. As a result, this practice is also known as doping in LECs.

The production of highly conductive regions results from the generation of doped zones, which are p-type at the anode and n-type at the cathode. The remaining applied potential, which is not used for charge injection from the electrodes, falls over the low-conductive intrinsic region between the doped zones, where light emission occurs. Current–voltage analysis, electrostatic potential measurement, and photoluminescence have all been used to confirm the presence of these doped layers in planar and sandwiched LECs [52–55]. Doped zones are known to quench excitons,

causing photoluminescence to decrease. When no precautions are taken and ion supply is not restricted, the p- and n-doped zones increase with operation time until they eventually collide. Due to increased exciton quenching by approaching doped regions, the exciton-to-photon conversion efficiency falls during this development process. The brightness of the LEC decreases as a result, and eventually no light is emitted [42]. Numerical modeling, experimental data, and a combination of the two provided fundamental insight into the doping kinetics during the creation of the p–i–n junction [56]. The electrical and ionic mobility, the applied bias voltage, and the thickness of the active layer have all been shown to influence the formation and migration of doping fronts [57]. The time it takes an ion to span approximately half of the electrode spacing was discovered to be directly connected to the turn-on time of LECs. The binding energy between anions and cations has been shown to be a crucial component in determining response time [38].

The fraction of electrons and holes that recombine to produce excitons (b), the exciton-to-photon production efficiency (w), and the number of photons that can escape the device or outcoupling efficiency calculated by 1/2n2 [58] determine the external quantum efficiency (EQE).

$$\mathrm{EQE}=\frac{b\varphi}{2n^2}$$

All electrons and holes recombine (b = 1) in LECs when the injection barriers are overcome [59]. The outcoupling efficiency is mostly determined by the device's design and the light generating zone. The former is predictable, but the latter is unpredictable and has been found to fluctuate over time [45,60]. That leaves φ as the most readily adjustable component. It's vital to remember that when an electron and a hole recombine, a singlet or a triplet exciton is created. According to statistics, 75 percent of excitons are triplet and 25% are singlet. Triplet excitons do not emit light at normal temperature in most organic materials. The effectiveness of fluorescent LECs is greatly limited by temperature. On the other side, phosphorescent emitters may gather light. Singlet and triplet excitons are both possible. Heavy metal is used in iTMCs. Elements like ruthenium or iridium that allow for a high degree of precision effective cross-system communication as a result, they are phosphorescent. structures that, theoretically, lead to considerably more efficient gadgets. φ is also affected by photoluminescent efficiencies. In thin film configurations, this can be rather high. However, as previously stated, the action of LECs leads to the creation of doped materials. Areas that expand with time, resulting in the partial quenching of the excitons, resulting in a decrease in φ. As a result, at the start of light emission, LECs have the maximum efficiency. Because the level of doping is determined by the current density used, device efficiency declines as current density rises. That explains why the maximum efficiencies have been found at low luminescence levels [61,62].

Apart from the active layer ingredients, pLECs and iTMC-LECs often have operating time scales that are many orders of magnitude different at room temperature. As a result, they've been classified and treated as two separate sorts of gadgets. Van Reenen et al. recently established that both types of devices exhibit performance transients, such as current, brightness, and efficacy [63]. This emphasizes the fact that pLECs and iTMC-LECs are two extremes of the same electroluminescent device class. Furthermore, because it has the same activation energy as ionic conductivity in the off state, it was determined that the ionic conductivity dominates the turn-on

time of polymer and iTMC-based devices. Extremes of an electroluminescent device class Furthermore, it. Apart from the active layer ingredients, pLECs and iTMC-LECs often have operating time scales that are many orders of magnitude different at room temperature. As a result, they've been classified and treated as two separate sorts of gadgets. Van Reenen et al. recently established that both types of devices exhibit performance transients, such as current, brightness, and efficacy [63]. This emphasizes the fact that pLECs and iTMC-LECs are two extremes of the same electroluminescent device class. Furthermore, because it has the same activation energy as ionic conductivity in the off state, it was determined that the ionic conductivity dominates the turn-on time of polymer and iTMC-based devices. The turn-on time of polymer and iTMC-based systems was found to be similar. Ionic conductivity is dominant in devices because it demonstrates the ionic conductivity in the off state has the same activation energy.

3. Introduction of Quantum Dots (QDs)

Quantum dots (QDs) are tiny crystals that can transport electrons and are produced by humans. When ultraviolet light strikes these semiconducting nanoparticles, they generate a rainbow of colors. Composites, solar cells, and fluorescent biological markers have all benefited from these manufactured semiconductor nanoparticles.

Quantum dots are semiconductor nanoparticles that were first manufactured in the early 1980s after being postulated in the 1970s. Quantum effects come into play when semiconductor particles are made tiny enough, limiting the energies at which electrons and holes (the lack of an electron) may exist in the particles. Because energy is proportional to wavelength (or color), the particle's optical characteristics may be carefully controlled based on its size. By manipulating the size of particles, they may be made to emit or absorb certain wavelengths (colors) of light.

Quantum dots are man-made nanostructures that, depending on their substance and form, can have a wide range of characteristics. They can be employed as active materials in single-electron transistors, for example, due to their unique electrical characteristics.

A quantum dot's attributes are controlled not just by its size, but also by its form, composition, and structure, such as whether it is solid or hollow. A reliable manufacturing technology that makes use of quantum dots' properties – for a wide range of applications in catalysis, electronics, photonics, information storage, imaging, medicine, or sensing – must be capable of producing large quantities of nanocrystals with the exact same parameters in each batch.

Nanocrystals might be a key building block for self-assembled functional nanodevices since some biological molecules are capable of molecular recognition and self-assembly.

QDs' atom-like energy states also contribute to unique optical features, such as a particle-size-dependent fluorescence wavelength, which is exploited to make optical probes for biological and medical imaging.

4. Quantum Dots (QDs) in Light-emitting electrochemical cells (LECs)

4.1 Introduction to Semiconductor Nanocrystals

Colloidal semiconductor nanocrystals (NCs) and solution-processed nanoscale crystals have been extensively studied in the last 30 years, not only for their scientific value, but also for their numerous technological applications, particularly in optoelectronics (e.g., display, lighting, and photovoltaics), as well as biological imaging and detection [64-70]. They're also known as quantum dots (QDs), because they have unique size-dependent electrical, optical, magnetic, and chemical capabilities that their bulk counterparts can't match [2]. The completely adjustable fluorescence emission of NCs, which covers the whole visible spectrum as a function of their size—Fig. 3 [64, 65]—is the most popular illustration of size-dependent properties of NCs. For optical devices to produce a crisp colored emission, size homogeneity is critical [65]. Semiconductor nanocrystals vary from their bulk counterparts in several ways. This shift is caused by quantum size effects [71], which are changes in the density of electronic energy levels as a function of size.

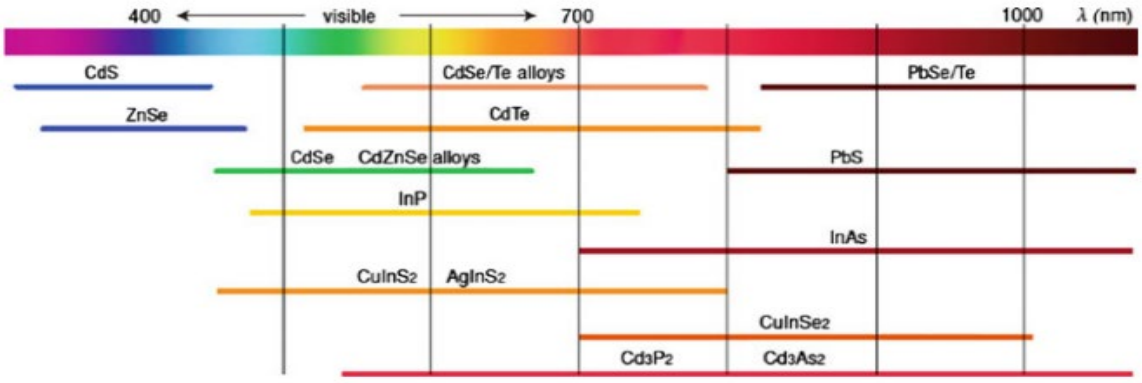

Fig.3: Spectral range of emission for the most widely studied types of semiconductor NCs [64]. Reprinted with permission from Ref. [64]. Copyright (2016) American Chemical Society

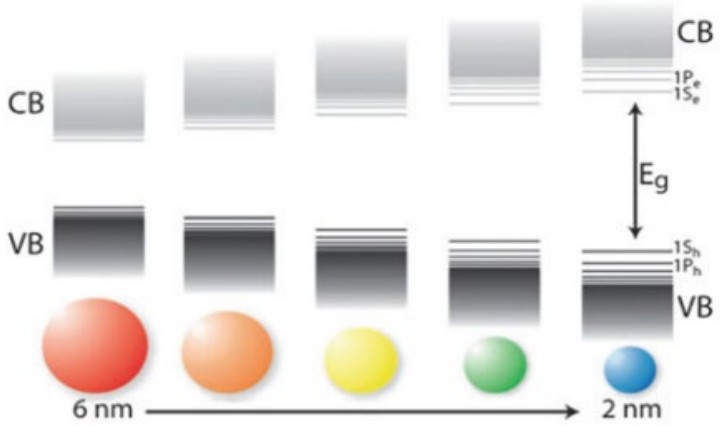

Fig.4: Schematic representation of the quantum confinement effect on the energy level structure of a semiconductor material [72]. Adapted from Ref. [72] with permission from the Royal Society of Chemistry

The energy gap widens as the size of the QD shrinks, resulting in a blue shift in the emission wavelength [72]. Due to quantum confinement, the continuous energy bands of the bulk material collapse into discrete energy levels—Fig. 4 The discrete structure of energy states leads to the discrete absorption spectrum of QDs, as opposed to their bulk counterparts, which have a continuous absorption spectrum [73].

4.2 Colloidal QDs

Colloidal QDs are made up of a tiny inorganic semiconductor crystal (1–10 nm) and an organic outer layer of surfactant molecules (ligands) that prevent the NCs from aggregating (Fig. 5). However, due to their high surface-to-volume ratio, a major portion of these materials have poor photoluminescence quantum yields (/), since they show surface-related trap states. As a result, photo produced charge carriers experience quick non-radiative relaxation pathways. To increase surface passivation, a shell of a second semiconductor was grown over the QD, which is known as a core/shell (CS) system. This approach improved fluorescence efficiency and photo-oxidation stability. Furthermore, by selecting appropriate core and shell materials, the emission wavelength may be readily modified [73].

The band alignment of CS systems is classified—see Figure 5-right: (i) Type-I CS NCs have a greater band gap between the shell and core materials. Because the band gap of the shell is thinner than the core, electrons and holes are confined in the core, resulting in a direct exciton; (ii) Reverse type-I CS NCs (Type-$I\frac{1}{2}$), where holes and electrons are partially or totally contained in the shell depending on shell thickness; (iii) Type-II CS NCs have a staggered energy level alignment, leading in the spatial separation of electrons and holes in distinct parts of the CS structure and the creation of an indirect exciton. In this instance, the shell material's valence band

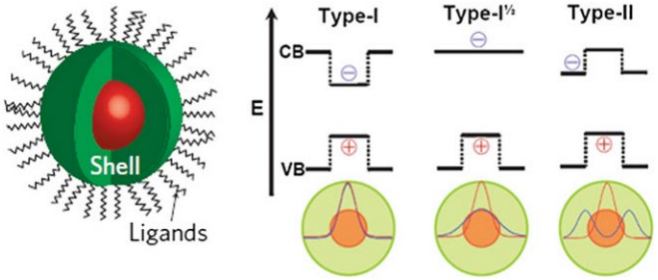

Fig.5: Left Schematic of a typical core–shell colloidal QD [67]. Right Schematic representation of the three limiting charge carrier localization regimes in core/shell semiconductor HNCs. The conduction and valence band edges (i.e., the LUMO and HOMO energy levels) are indicated by CB and VB, respectively. The plus and minus signs represent the charge carriers (hole and electron, respectively) [71]. Figure 5 left is adapted by permission from Macmillan Publishers Ltd: Nat. Photon [67]. Copyright 2013. Figure 5 right is reproduced from Ref. [71] with permission from the Royal Society of Chemistry.

or conduction band edge interacts with the core's band gap [71, 73]. We'll concentrate on Type-I CS NCs in this chapter. We recommend the reader to these sources [67, 71] for different forms of CS NCs.

4.3 Type -I Core-Shell NCs

The shell is utilized to passivate the core's surface to improve its optical qualities in this form of NC. The shell helps to isolate the optically active core from its surrounding medium. Water and oxygen molecules, which induce a change in the immediate environment of the NCs and hence modify the optical characteristics, are not able to impact the core in this way. As a result, CS NCs outperform basic NCs in terms of photodegradation stability. Another benefit of covering the core NCs with a shell is that it reduces surface dangling bonds, which lowers the Ø since these bonds function as charge carrier trap states [72, 73].

The temperature for shell development (T2) is critical in order to avoid nucleation of shell material and uncontrolled ripening of the core NCs. CS systems are generally synthesized in a two-step procedure: I synthesis and purification of core NCs and (ii) the shell growth reaction—Fig. 6 As a result, T2 is often lower than the temperature at which core NC synthesis occurs (T1). Furthermore, in order to achieve the necessary shell thickness, the concentration of the core NCs is an important factor in the synthesis of NCs. Drying the material and weighing it yields this information [73].

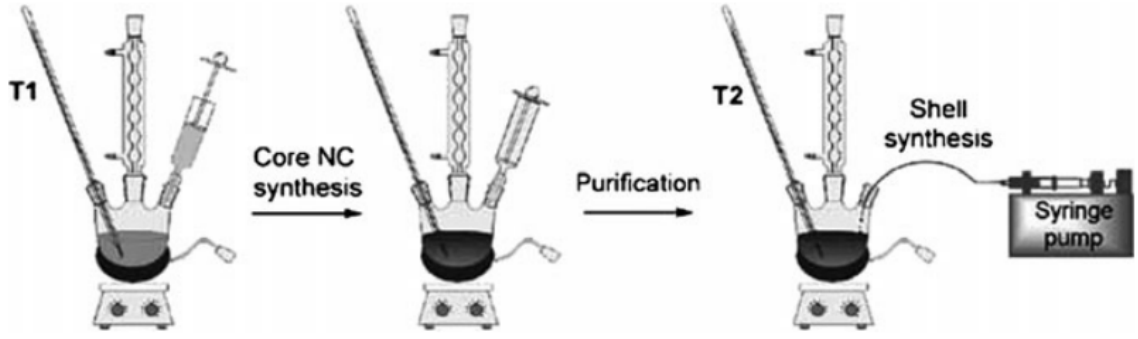

Fig.6: Two-step synthesis of core/shell nanocrystals [10]. Reproduced from Ref. [10] with permission from John Wiley and Sons © 2009 Wiley-VCH GmBH & Co. KGaA, Weinheim.

4.4 CdSe-Based QDs—QDs Used in LECs

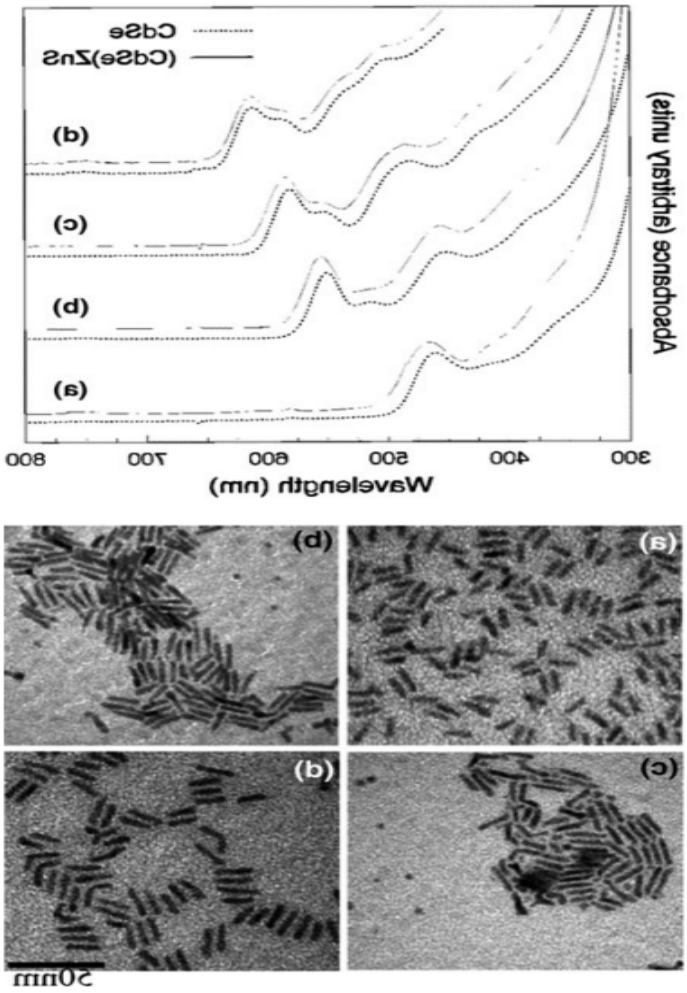

Fig.7: Top Absorption spectra for bare (dashed lines) and 1–2 monolayer ZnS overcoated (solid lines) CdSe dots with diameters measuring a 23, b 42, c 48, and d 55 Å. The absorption spectra for the (CdSe)ZnS dots are broader and slightly red-shifted from their respective bare dot spectra [75]. Bottom TEM images of rod and core/shell nanorod samples. a Rods 22 4 nm. b–c Core/shell nanorod samples that were grown from rods have shown in (a), with shell thicknesses of 1.7 and 3.5 monolayers (ML), respectively. Dots can be seen in both samples. d the sample is shown in (c) after separation. The dots were removed. Figure 7- top is reprinted with permission from Ref. [76]. Copyright (1997) American Chemical Society. Figure 7- bottom is reprinted with permission from Ref. [76].

Type-I CS QDs, notably CdSe/ZnS QDs from II-VI SC NCs, have been the most studied colloidal semiconductor NCs to date [73]. Hines et al. first described their method, in which CdSe NCs were coated with 1–2 monolayers of ZnS, resulting in Ø Yield of 50%. By infusing a combination of organometallic precursors diethylzinc and hexamethyldisilathiane, commonly known as is(trimethylsilyl)sulfide, S(TMS)2 [74], the ZnS shell was grown at a high temperature (300 °C). Dabbousi et al. published a follow-up report not long after this first one. [75] exhibited extremely luminous CdSe/ZnS NCs with Øs of 30–50% at room temperature, encompassing the majority of the visible spectrum from blue to red—Fig. 7-top. Additionally, since the original publication of their synthesis by Peng et al., the nanorods have piqued curiosity due to their linearly polarized emission feature, which makes them interesting as prospective laser materials compared

to spherical dots—Fig. 7-bottom [76, 77]. We direct the reader to the following in-depth reviews [73, 75] because these NCs have been the most explored.

CdSe/CdS CS QDs, which have a different band orientation, are another intriguing system. A substantial band offset for the holes is paired with a relatively modest band offset for the electrons in this form of QD. Peng et al. [78] demonstrated the production of epitaxially grown CdSe/CdS CS NCs with shells as thick as three monolayers and core sizes ranging from 23 to 39 mm. Later, the formation of CdSe/CdSe CS NCs was shown using the sequential ion layer adsorption and reaction (SILAR) approach based on alternating injections of the Cd and S precursors into the CdSe NCs solution. By building a very thick inorganic shell, this process has been expanded to the production of 'giant' CdSe/CdS NCs with a shell thickness of 6 nm in order to render their optical properties—namely, photobleaching and blinking—independent of their surface chemistry and chemical environment [79].

4.5 Perovskites

In the last few years, inorganic–organic halide perovskites have ushered in a new age of low-cost, high-efficiency solar cells. They've already demonstrated photovoltaic efficiencies of over 22% [83], making it the highest-performing solution-processed solar cell ever. The unexpected breakthrough and rapid evolution of this family of materials has energized not only the photovoltaic community, but also the lighting community's efforts to develop devices using low-cost, readily available constituents, such as methylammonium lead bromide (CH3NH3PbBr3) and its analogs [84–85]. The similarities to the gold standards of crystalline silicon and GaAs, such as a sharp band gap close to the ideal, high absorbance—Fig. 8-top, low exciton binding energy with the excited state composed primarily of free carriers—Fig. 8-bottom, near-perfect crystalline film formation with very low defect densities, balanced electron–hole transport, and excellent charge cation transport, have contributed to the success of inorganic–organic lead halide perovskites [85].

They have been widely researched in crystalline families of hybrids prior to their current investigation in photovoltaics. Organic–inorganic hybrid perovskites have advantageous features that may be exploited in a broad variety of semiconductor applications [90] because to the inclusion of both organic and inorganic elements inside a single crystalline structure.

The stoichiometry of the archetypal perovskite is cubic ABX_3, with A being an organic cation, B being a divalent metal, and X being a halide anion. While A is generally methylammonium $(CH_3NH_3)^+$ or formamidinium $(CH(NH_2)_2^+)$, B is Pb^{2+}, and X is frequently Cl^-, Br^-, or I^-. As illustrated in Fig. 9 [28–31], the metals are usually in a 6-fold coordination and are surrounded by an octahedron of halide anions, as well as organic cations in a 12-fold cuboctahedral coordination.

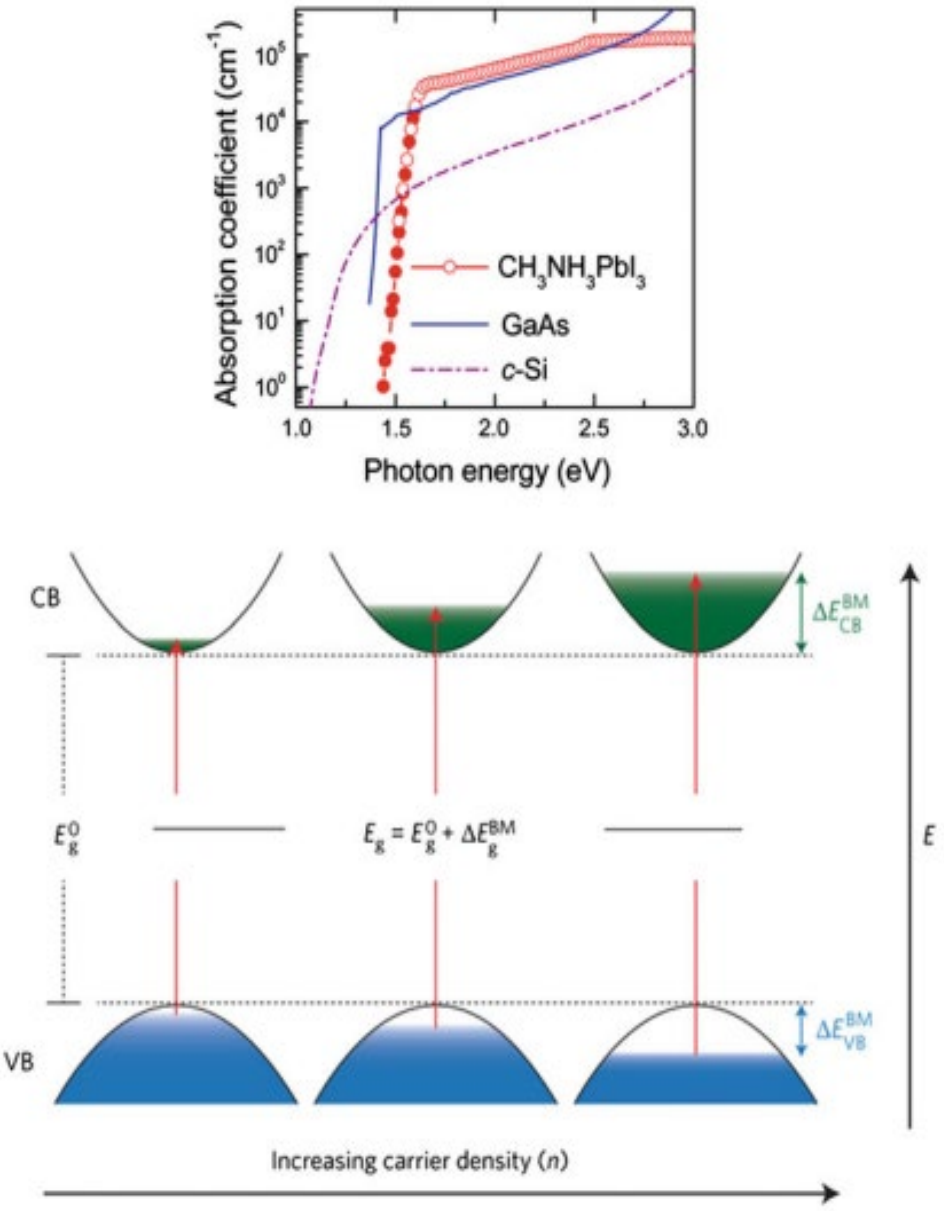

Fig.8: Top Effective absorption coefficient of a CH3NH3PbI3 perovskite thin film compared to other typical photovoltaic materials, including amorphous silicon (a-Si), GaAs, CIGS, CdTe, and crystalline silicon (c-Si) [88]. Bottom Schematic representation of the Burstein–Moss effect showing the contribution from both electrons in the conduction band (CB) and holes in the valence band (VB) due to their similar effective masses [89]. Figure 8-top is reprinted with permission from Ref. [88]. Copyright (2014) American Chemical Society. Figure 8-bottom is adapted by permission from Macmillan Publishers Ltd: Nat. Photon [89].

In addition to hybrid organic–inorganic perovskites, wholly inorganic equivalents have been demonstrated by substituting the organic cation with an inorganic cation—Cs+, resulting in enhanced structural stability [91]. The composition of perovskites is clearly so variable that their optical and electrical characteristics may be readily altered and modified. Apart from

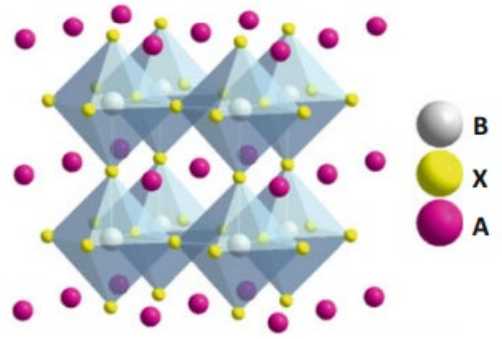

Fig. 9: Single unit cell of an ABX3 perovskite crystal, where A is an organic cation, B is a divalent metal, and X is I, Br, or Cl

photovoltaics (PV), these materials have been employed in a variety of optoelectronic applications such as light-emitting diodes (LEDs), photodetectors, and lasers [92-93].

4.6 Perovskite Nanostructures

Perovskites have low energy barriers for forming organic–inorganic hybrid structures, allowing them to form crystalline phases by simply mixing and grinding the precursor salts at room temperature, as opposed to inorganic perovskite oxides, which require elevated temperatures (>600 °C), making them incompatible with most optoelectronic substrates. As a result of their ease of synthesis, they have already surpassed classic inorganic oxides [95, 99, 100]. Their morphology (from 3D to 0D) and size (from mm to nm range) may readily be adjusted by carefully adjusting reaction parameters such as temperature, solvent, and ligands (Fig. 10) [93, 101–104]. The Nano structuring of materials has become intensively explored in a short time due to the simplicity of preparing a large variety of nanostructured perovskites and the existence of exceptional characteristics at the nm scale [95]. Different optical features, such as adjustable PL emission with various sizes due to quantum size effects, may be easily achieved by varying reaction conditions [105-106]. Another notable aspect of hybrid perovskite is that, unlike traditional semiconductor NCs, they do not require additional surface passivation to produce a high Ø Surface ligands' dangling bonds do not appear to play a role in PL emission, resulting in values that are already close to 100% without additional optimization [107-108].

In contrast to semiconductor QDs, they do not exhibit spectrum broadening due to high surface trap concentrations or size dispersion. Furthermore, no change in optical band gap was detected at increased temperatures. This is critical for maintaining color purity in light-emitting devices [108]. Perovskite nanostructures can be used in light-emitting diodes (LEDs) [102, 109], as well as lasing and photodetectors [110, 111].

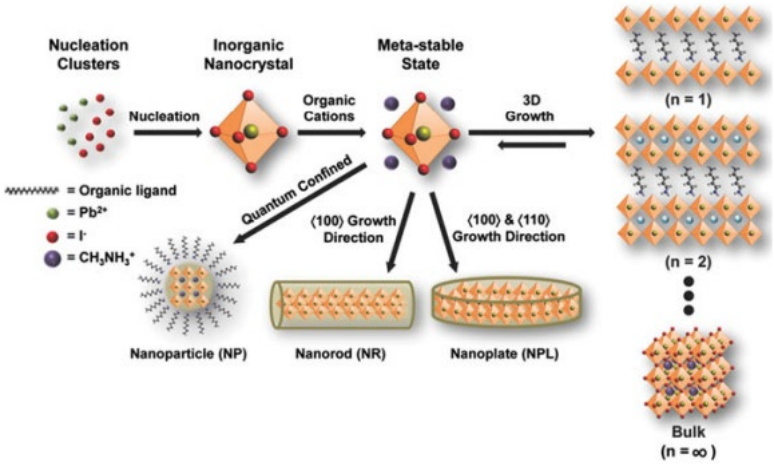

Fig. 10 Schematic representation of the hybrid-perovskite phase formation and the resulting morphologies [106]. Adapted from Ref. [106] with permission from John Wiley and Sons © 2016 Wiley-VCH GmBH & Co. KGaA, Weinheim

4.7 Synthesis of Perovskite NCs

In the production of hybrid organic–inorganic perovskites, the ligand-assisted re-precipitation technique (LARP) is commonly utilized. To stabilize the produced particles, a combination of a polar solvent and inorganic lead and ammonium halide salts (PbX_2 and MAX) is injected into a nonpolar poor solvent in the presence of ligands [95, 96, 97]. With $CH_3NH_3PbBr_3$ NCs, Schmidt et al. [93] pioneered this synthesis scheme—Fig. 11-top.

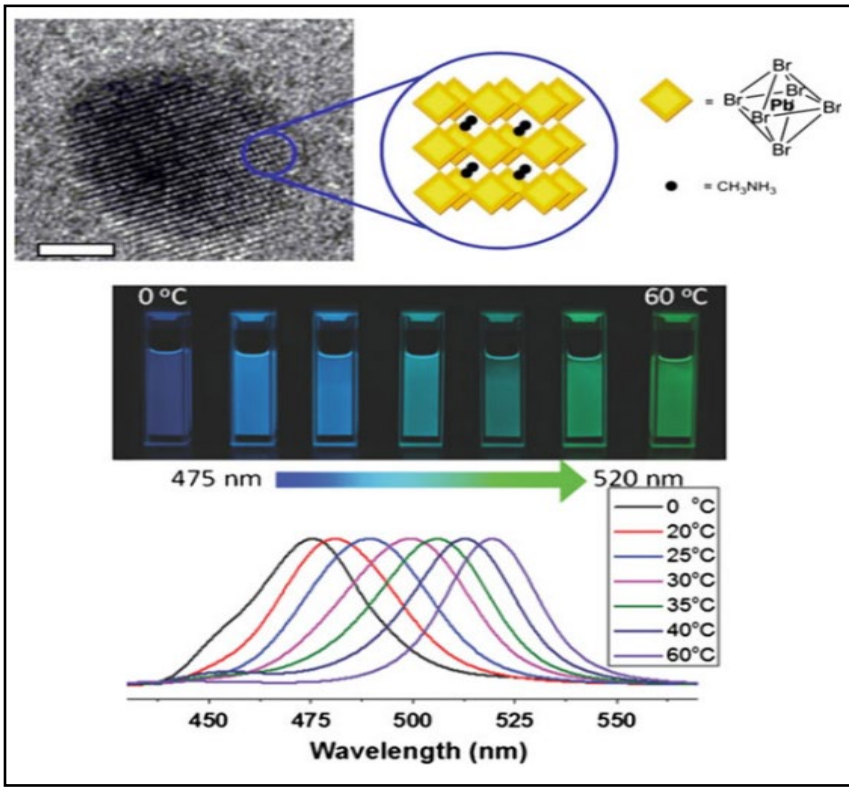

Fig. 11 Top HRTEM image of an isolated perovskite nanoparticle (scale bar 2 nm) and schematic representation of an array of corner sharing MX6 octahedra confined in the three dimensions due to the organic capping [93]. Bottom photograph of colloidal solutions in toluene under UV lamp excitation (k = 365 nm) and PL spectra tunability over the range of wavelengths indicated [113]. Figure 11-top is reprinted with permission from Ref. [93]. Figure 11-bottom is reprinted from Ref. [113] with permission from John Wiley and Sons.

The produced nanoparticles (NPs) emitted a bright-green PL emission at 527 nm with a Brightness of around 20%. Huang et al. also demonstrated the quantization impact of $CH_3NH_3PbBr_3$ NPs by adjusting the reaction temperature (Fig. 11-bottom). This also enables for an increase in Brightness of 74 to 93 percent, with emission peaks spanning the wavelength range of 475 to 520 nm [112].

Despite its high Density and colloidal stability for several months, perovskite NPs are unstable in polar solutions [113]. They may, however, be produced without the use of polar solvents by performing the reaction in a high boiling nonpolar solvent (1-octadecene) in the presence of coordinating ligands oleylamine and oleic acid [114]. This novel approach offers a different way to make NCs, even if their Ø is lower than previously described $CH_3NH_3PbBr_3$ NCs.

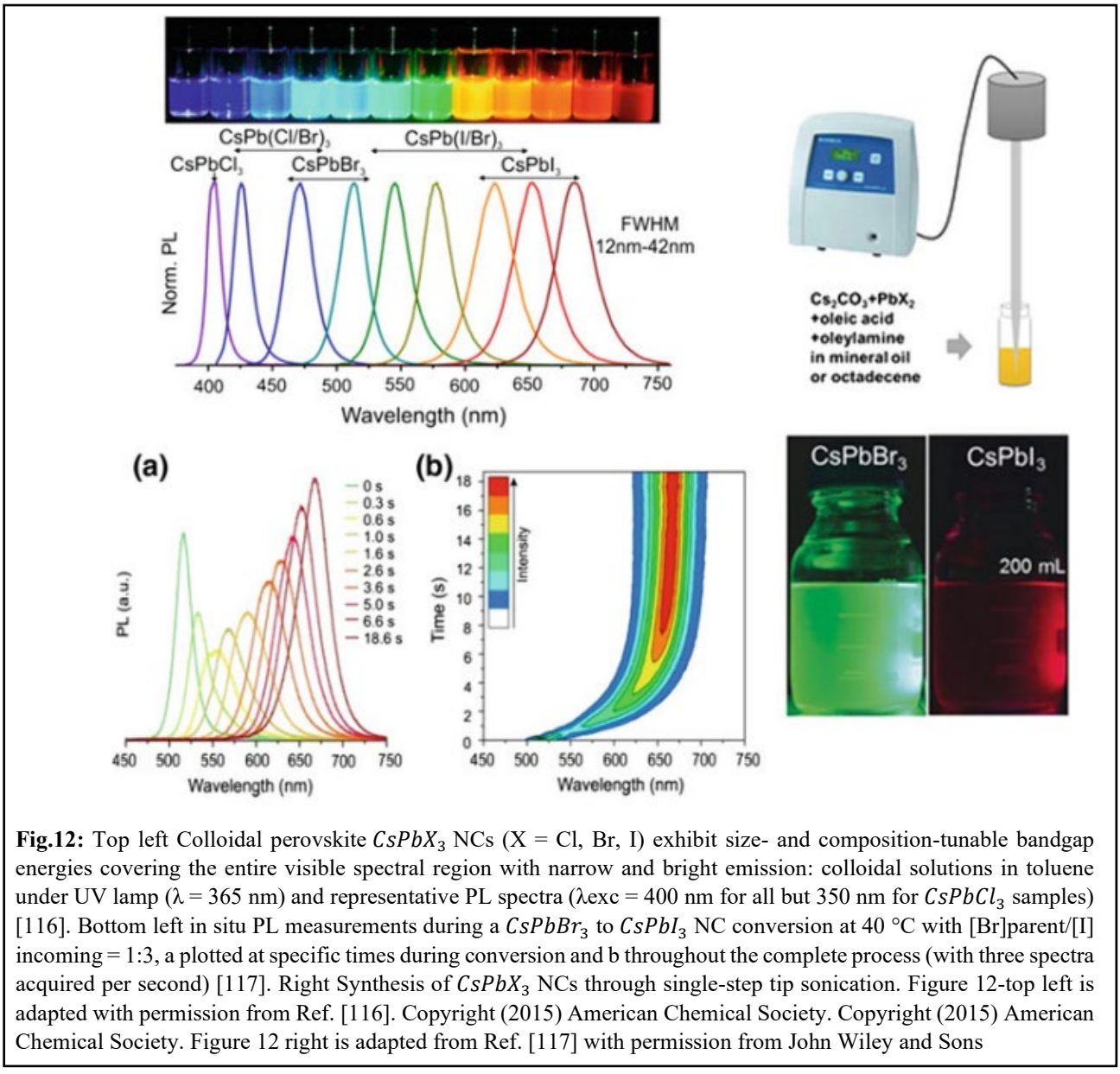

Fig.12: Top left Colloidal perovskite $CsPbX_3$ NCs (X = Cl, Br, I) exhibit size- and composition-tunable bandgap energies covering the entire visible spectral region with narrow and bright emission: colloidal solutions in toluene under UV lamp (λ = 365 nm) and representative PL spectra (λexc = 400 nm for all but 350 nm for $CsPbCl_3$ samples) [116]. Bottom left in situ PL measurements during a $CsPbBr_3$ to $CsPbI_3$ NC conversion at 40 °C with [Br]parent/[I] incoming = 1:3, a plotted at specific times during conversion and b throughout the complete process (with three spectra acquired per second) [117]. Right Synthesis of $CsPbX_3$ NCs through single-step tip sonication. Figure 12-top left is adapted with permission from Ref. [116]. Copyright (2015) American Chemical Society. Copyright (2015) American Chemical Society. Figure 12 right is adapted from Ref. [117] with permission from John Wiley and Sons

It is also feasible to substitute an inorganic cation (Cs^+) for the organic cation. The color-tunable $CsPbX_3$(X = Cl, Br, I) NCs are made using a hot injection process at high temperatures (140–

200 °C). For the first time, Protesescuet al. reported the synthesis of these NCs by injecting the Cs-oleate precursor into a PbX_2 solution in non-coordinating solvents and ligands at high temperatures in a N_2 environment. Because the synthesized NCs have a high Bohr radius of roughly 12 nm determined for $CsPbX_3$ (Fig. 12-top left) [116], they showed quantum confinement. Several groups then showed post-synthetic chemical changes, ion-exchange, of these NCs in order to use halide exchange as an additional tool to modify the optical and structural properties of NCs in a quick and easy way—Fig. 12-bottom left [117, 118]. Tong et al. has demonstrated a flexible and single-step technique for the large-scale synthesis of $CsPbX_3$ NCs at room temperature, whereas all previous synthesis methods have relied on high temperatures (Fig. 12-right). Their approach involves tip sonication of mixes of the respective precursor salts and capping ligands in a nonpolar solvent under ambient circumstances, which results in highly luminous NCs (Ø s up to 90%) that cover the visible spectrum (400–700 nm) [119].

In order to modify the form of the NCs, crystal development in one direction can be blocked in addition to changing the size of the NPs [119, 120]. Nanoplatelets can be made by altering the ratio of precursors and ligands [107, 116] or regulating the reaction temperature [118]. Depending on the thickness of the perovskite unit cells (Fig. 13-left), quantum confinement effects are also evident [117]. In addition, Zhang et al. [118] demonstrated that $CsPbX_3$ nanowires may be made by adjusting the reaction time—Fig. 13-right.

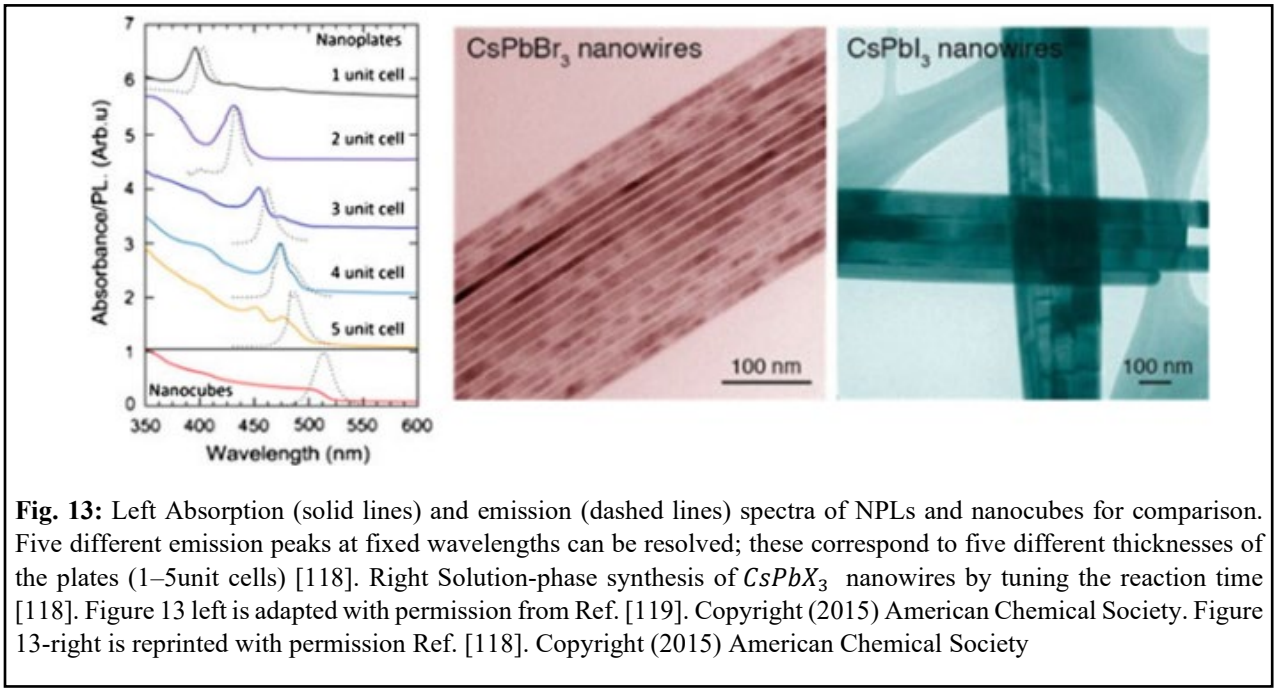

Fig. 13: Left Absorption (solid lines) and emission (dashed lines) spectra of NPLs and nanocubes for comparison. Five different emission peaks at fixed wavelengths can be resolved; these correspond to five different thicknesses of the plates (1–5unit cells) [118]. Right Solution-phase synthesis of $CsPbX_3$ nanowires by tuning the reaction time [118]. Figure 13 left is adapted with permission from Ref. [119]. Copyright (2015) American Chemical Society. Figure 13-right is reprinted with permission Ref. [118]. Copyright (2015) American Chemical Society

A self-template-directed reaction of Pb-containing nanowires with HBr and CH3NH3Br in solution at room temperature exhibited porous $CH_3NH_3PbBr_3$perovskite nanowires [119].

5. Applications of NCs into LECs

5.1 Core-Shell QDs Emitters for LECs

High color tunability due to size-tunable band gaps, high Brightness, and strong stability highlighted CS NCs' promise as light-emitting materials in a number of optoelectronic applications, such as light-emitting electrochemical cells (LECs). By combining QDs into a single polymer layer, Bader et al. reported the first LECs based on QDs that emit virtually pure emission from the CdSe/ZnS QDs, regardless of applied voltage.

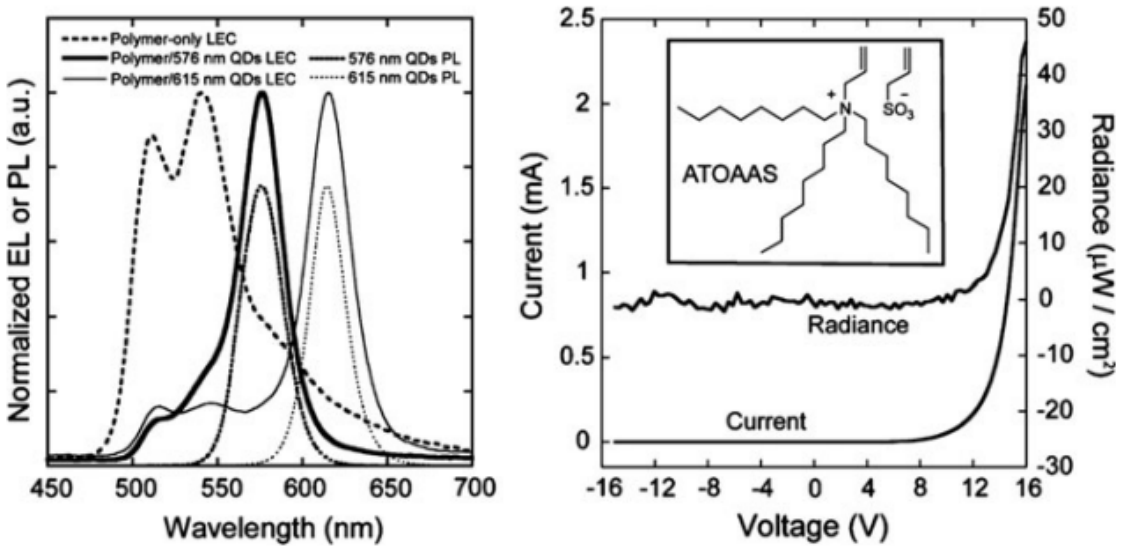

Fig. 14: Left Normalized EL spectra of three LEC devices presented in this study, as well as the PL spectra of the two QD materials used. Right Representative current–voltage and radiance– voltage curves of QD-LECs. Inset The chemical structure of ATOAAS, the source of counter ions used in these QD-LECs [120]. Figure 14 is adapted with permission from Ref. [121]. Copyright (2011) American Chemical Society

The light-emitting film, composed of the PF/PPV copolymer–poly [(9,9-diocty12,7-divinylene-fluorenylene)-alt-co-{2-methoxy-5-(2-ethyl-hexyloxy)-1,4 phenylene}], CdSe/ZnS CS QDs, and the polymerizable ionic liquid allyltrioctylammonium allylsulfonate (ATOAAS) (Fig. 14-inset) as the source of counterions, was sandwiched between a patterned indium tin oxide (ITO) substrate and gold electrodes. After adding QDs to the LEC, the spectra switched to an intense narrow peak centered at the PL of the QDs, whereas the spectrum of the polymer-only devices revealed wide electroluminescence (EL) (Fig. 14-left). At 16 V, the QD-LECs had a maximum brightness of

Mass ratio of QDs (576 nm:615 nm)	CIE coordinates (*x*, *y*)	Photot of device pixel
8:0	(0.46, 0.51)	
6:2	(0.49, 0.47)	
4:4	(0.50, 0.46)	
2:6	(0.53, 0.43)	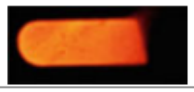
0:8	(0.55, 0.40)	

Table.1: Characterization of color in Multi-QD-LECs [120]. Table 1 is reprinted with permission from Ref. [120]. Copyright (2011) American Chemical Society

40–50 lW/cm2 (200–300 cd/m2)—Fig. 14-right. Table 1 [120] shows how they mixed varied ratios of two distinct sizes of QDs to exhibit fine color control.

Qian et al. later demonstrated just color saturated EL from QDs, with no additional emissions from the polymer host or electrolyte. They created the devices by combining various sizes of CdSe/CdS CS QDs with PVK and the ionic liquid 1-butyl-3-methylimidazolim hexafluorophosphate (BMIM-PF6). To avoid creating an insulating barrier with lengthy alkyl chains of QDs, they first used a ligand-exchange method. The QDs were miscible with the ionic liquid after this treatment, allowing for increased charge injection and mobility. They then presented blue, green, orange, and red QD-LECs, with orange QD-LECs having a Bmax of about 1000 cd/m2 —Fig. 14-top left and bottom left — and blue counterparts having the lowest brightness of 18 cd/m2 at 10 V —Table 2. Finally, in order to create white EL, multiple mass ratios of red:green:blue (R:G:B) QDs were examined, and the ratio of 1:16:7 was determined to be the optimum (Fig. 14-right). Green QDs have the greatest concentration in the blended film due to their low QY [121].

Frohleiks et al. recently demonstrated hybrid LECs made up of CdSe/CdS QDs and an Ir-based ionic transition metal complex (iTMC) (Fig. 16). Because there is a scarcity of brilliant and long-term stable emitter materials for diverse colors, the scientists wanted to broaden the emission color of iTMC-LECs. Both red QDs and yellow iTMC sources emitted light, according to the researchers. Charge carriers were introduced into both light-emitting species, allowing white light to be produced using QDs with various band gaps. Furthermore, because the extra QD layer improves electron injection into the active LEC layer, the device turned on faster and had higher brightness and efficiency values [123].

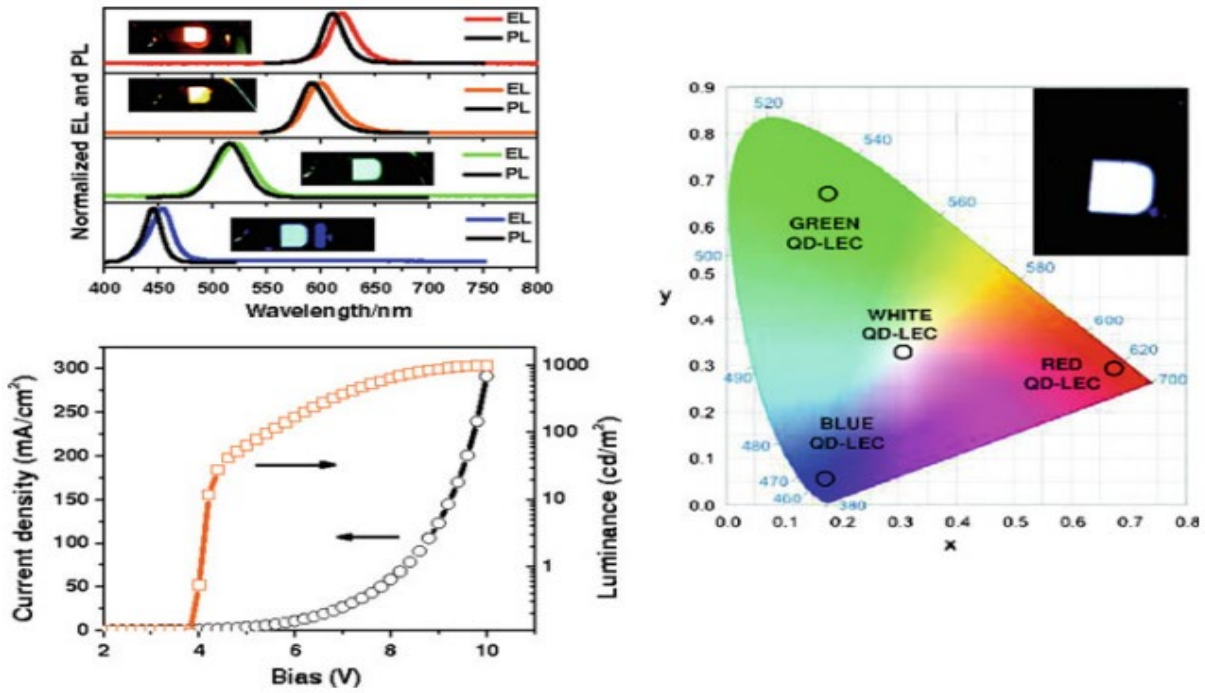

Fig. 15: Top left Normalized emission spectra of solution photoluminescence and QD-LECs electroluminescence. Inset photograph of a typical device (pixel size, 6 mm2). Bottom left Representative current density–voltage–luminance curves of the QD-LECs. Right CIE chromaticity diagram indicating the color of blue, green, red, and white QD-LECs. Inset photograph of a white QD-LEC in operation with 10 V of applied forward bias with CIE (0.33, 0.33) [121]. Adapted from Ref. [121] with permission from John Wiley and Sons © 2014 Wiley-VCH GmBH & Co. KGaA, Weinheim

QDs	V_{on} (V)	EL_{max} (nm)	B_{max} (cd/m^2)	Eff_{max} (cd/A)	PE (lm/W)	CIE (x/y)
Red	2.0	620	581	1.5	1.0	(0.67/0.33)
Orange	3.8	600	995	1.9	1.3	(0.59/0.38)
Green	3.8	520	208	1.2	0.6	(0.18/0.65)
Blue	4.0	453	18	0.4	0.6	(0.16/0.06)

Table.2: Table adapted from Ref. [121]. Note The terms Von, ELmax, Bmax, Effmax, PE, and CIE refer to turn-on voltage, maximum of the electroluminescence spectrum, maximum efficiency, maximum power efficiency, and x/y CIE color coordinates, respectively. The definition of these terms is provided in Chap.

Although the results of CS QDs-based LECs are equivalent to those of finely controlled multilayer LED devices, [122] there are still issues with this type of QDs that must be solved. The substantial fall in their Brightness as a result of ligand-exchange, which is an essential step for lighting applications [123], is one example of this sort of QDs' fundamental restriction. Another deficit of CS NCs is the low efficiency of blue-emitting nanoparticles—Table 2—due to their low Ø. They also have considerable sub-band gap

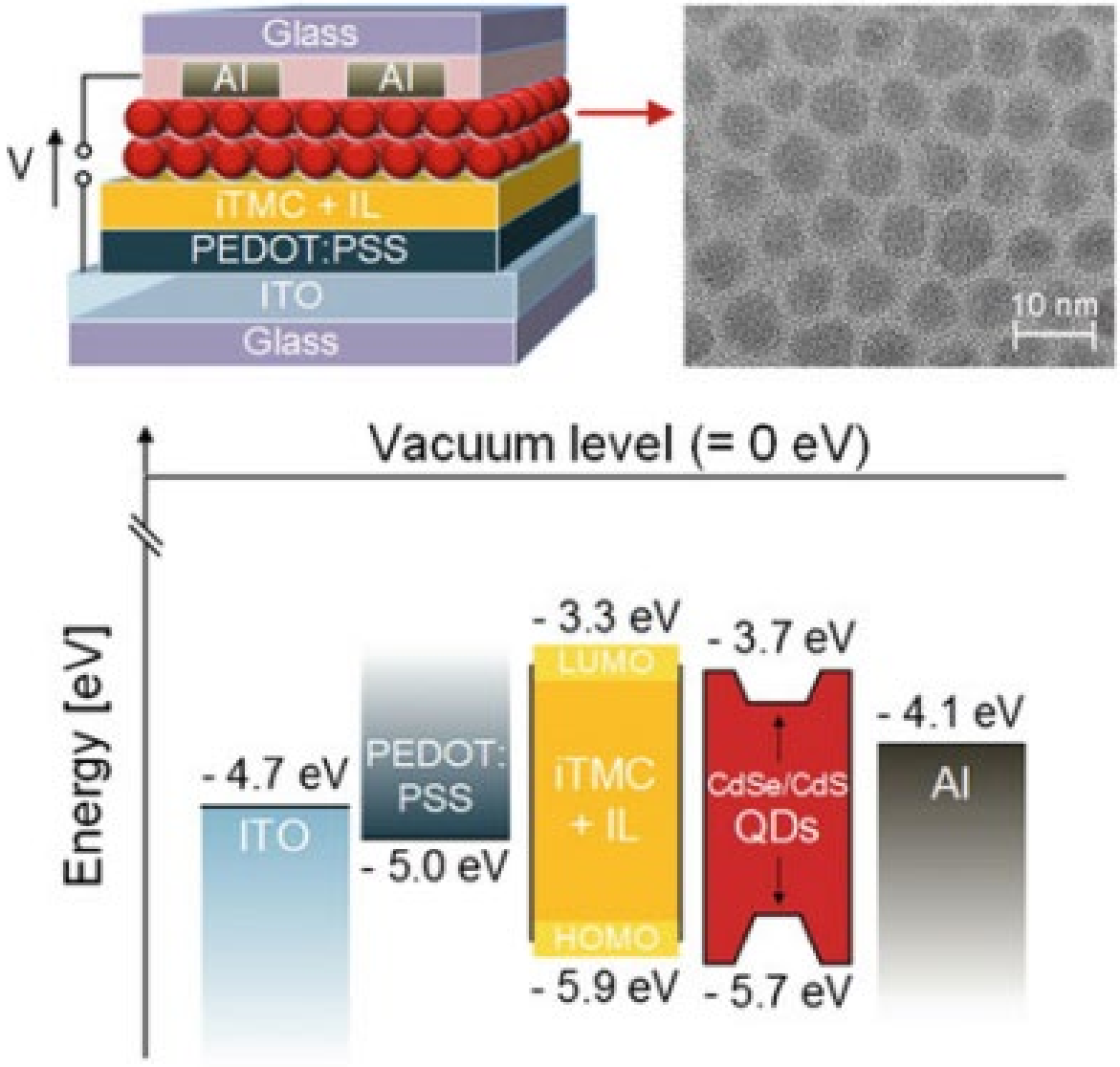

Fig.16: Top left Schematic of the QLEC device design. Top right TEM image of CdSe/CdS core– shell QDs. Bottom Schematic of simplified energy level diagram for QLEC [121]. Figure 16 is adapted with permission from Ref. [121]. Copyright (2016) American Chemical Society

flaws, which restrict the device's maximum performance. These disadvantages, on the other hand, are absent in freshly produced perovskites. As a result, it is envisaged that its employment in lighting applications would result in the manufacture of highly efficient and low-cost devices [123].

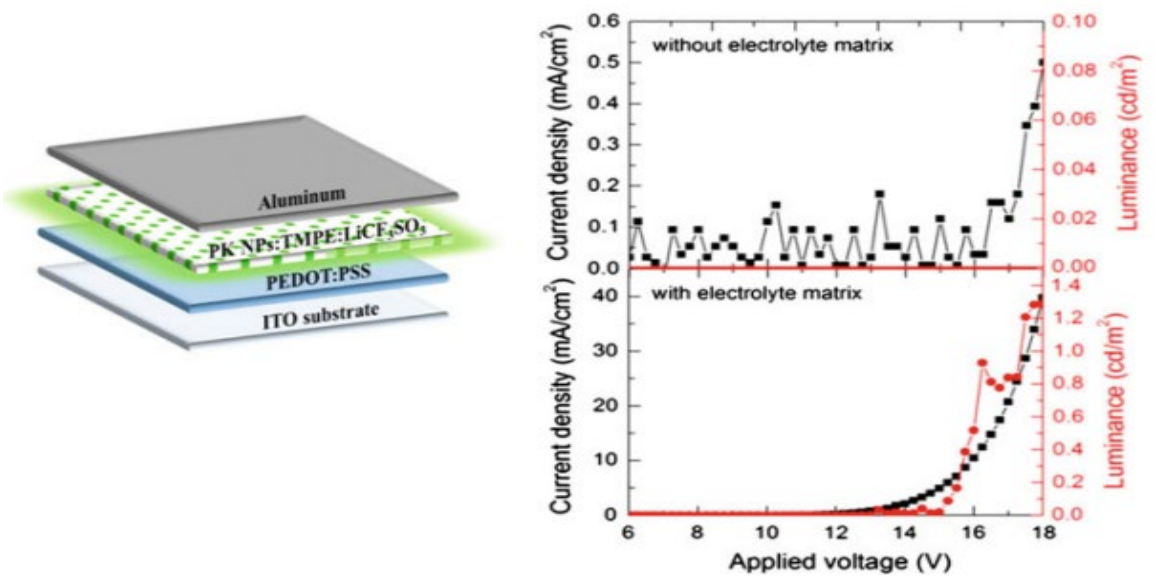

Fig.17: Left Illustration of device architecture employed in this work. Right Luminance (red circles)—current density (black squares) versus applied voltage of ITO/PEDOT:PSS (100 nm)/ MAPbBr3 NPs without electrolyte matrix (50−70 nm) and with electrolyte matrix (100–120 nm)/ Al (90 nm) devices [123]. Figure 17 is adapted with permission from Ref. [123].

5.2 Perovskite Emitters for LECs

Perovskite NCs are great candidates for use in LECs because of their easy and low-cost production, as well as their high Ratio Ø of 90% from red to blue emission. Using the absence of ligand-exchange processes in perovskite NPs, Aygüler et al. developed the first LECs based on MAPbBr3 perovskite NPs with a brightness of 1–2 cd/m2 at low driving currents— Fig. 17-left. The scientists also created a spray-coating-based deposition methodology, bringing this technology closer to large-scale applications. They also demonstrated the importance of the electrolyte matrix in device behavior, demonstrating that devices without this component had no visible luminance, but those with the electrolyte matrix had a lower injection voltage—Fig. 17-right.

Furthermore, the devices were studied using both constant voltage and pulsed current driving methods, demonstrating that LECs based on Ps had a similar behavior [124]. Using electrochemical impedance spectroscopy, Puscher et al. investigated electrolyte-free LECs based on MAPbBr3 NPs. Their findings revealed that the dynamic device behavior under applied bias is linked to ionic species movement and rearrangement, validating the anticipated LEC behavior for these systems [124].

In addition to its NPs, LECs have been shown with bulk perovskites. In a structure of bulk MAPbI3 sandwiched between two high work function electrodes of ITO/PEDOT:PSS and

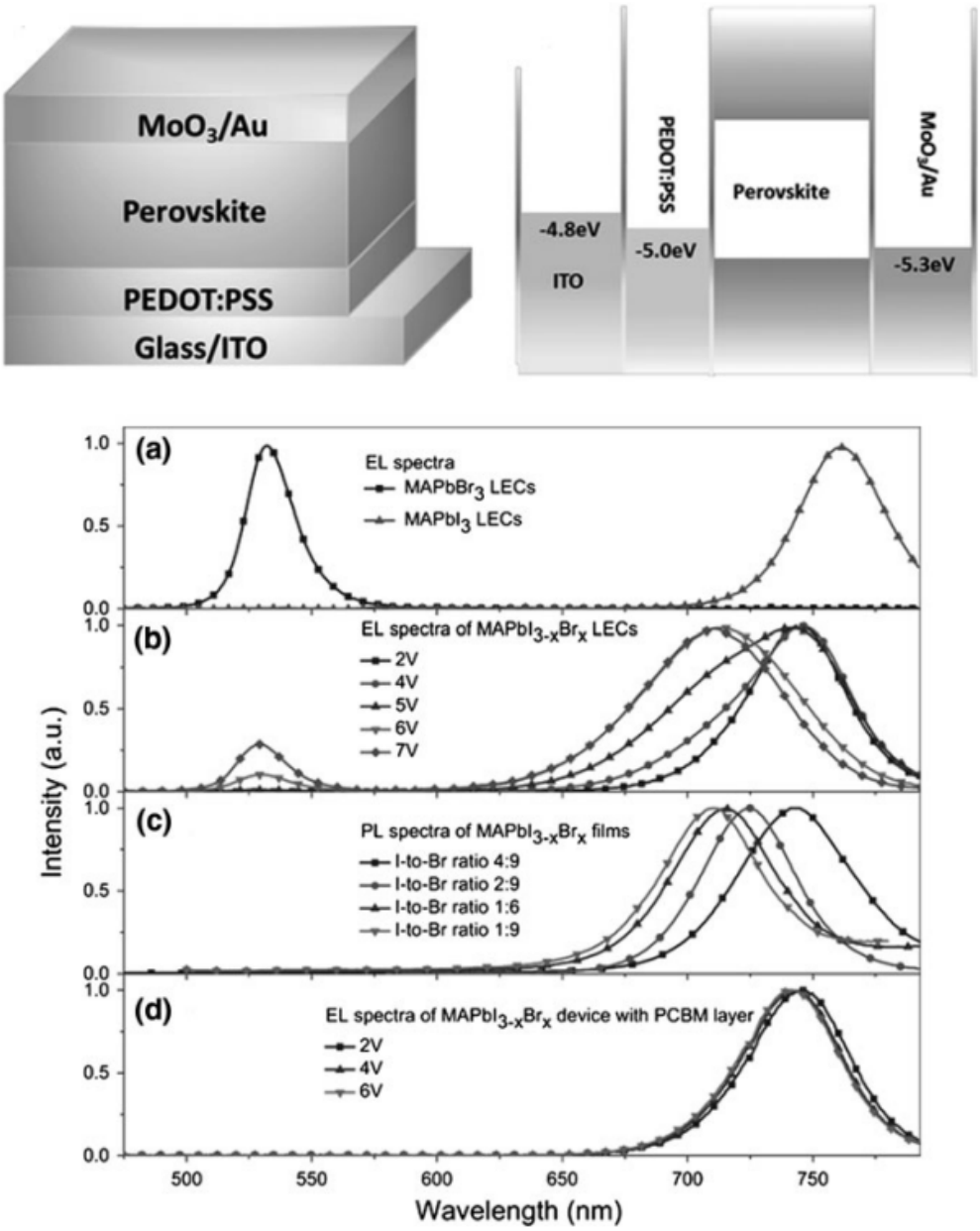

Fig. 18: Top left Device structure. Top right Energy level diagram of the materials. Bottom EL and PL spectra of bromide perovskite and mixed iodide–bromide perovskite: a EL spectra of MAPbI3 and MAPbBr3 in the LECs of ITO/PEDOT:PSS/Perovskite/MoO3/Au. b EL spectra of the mixed perovskite MAPbI3−xBrx in the LECs of ITO/PEDOT:PSS/Perovskite/MoO3/Au at different biases. c PL spectra of the mixed perovskite MAPbI3−xBrx with different I-to-Br ratios. d EL spectra of the mixed perovskite MAPbI3−xBrx in the device ITO/PEDOT: PSS/Perovskite/PCBM/Au at different biases [123]. Adapted from Ref. [123] with permission from John Wiley and Sons.

MoO_3/Au with work functions of 5.0 and 5.3 eV, respectively, Zhang et al. proved that organic–inorganic halide perovskites are solid electrolytes with mixed ionic and electronic conductivity—Fig. 17-top. The ionic conductivity of MAPbI_3 is on the order of 10^{-8} S cm^{-1}, according to their impedance spectroscopy analysis, and the collected ions at the interface are the cause of the

huge capacitance (≈100 μF cm^{-2}). The MAPbI_3 devices emitted infrared emission with a peak at 761 nm, whereas the $MAPbBr_3$ counterparts emitted green EL. Furthermore, in $(MAPbI_3)_{-x}Br_x$ based LECs, the change in EL with applied voltage suggested that I^{-1} ions migrate in the perovskite during operation— Fig. 18 bottom [125]. Finally, the inclusion of high work function electrodes in this basic device configuration increases the possibility for evolving perovskites into efficient and color-tunable light emitters for low-cost lighting applications. Finally, the inclusion of high work function electrodes in this basic device configuration increases the possibility for evolving perovskites into efficient and color-tunable light emitters for low-cost lighting applications.

6. Conclusion

The fast development of low-cost lighting applications based on LEC technology confronts a number of significant obstacles, including restricted color availability, irreversible device deterioration during operation ("self-killing"), and delayed turn-on/electrical reaction time. Hybrid QD-LECs, QLECs, and PeLECs are potential approaches to overcoming the first hurdle and realizing brilliant and steady large-area light-emitting devices in a variety of readily adjustable hues. The notion of combining the easy-to-process, flexible "single-layer" device architecture of LECs with the great resilience and color variation of classic colloidal and perovskite QDs and nanocrystals came closer to reality with the first proof-of-concept hybrid devices. Flexible, transparent, color-tunable, and white light-emitting devices were exhibited, indicating that this new technology has a lot of promise. Furthermore, the notion of decoupling light emission from charge transfer inside LECs by introducing robust and brilliant light-emitting species in QLECs and PeLECs might be the proper route to tackle the classic LECs' "self-killing" problem during operation. Within the new hybrids, the devices' delayed response time and distinctive timedependent behavior persist. In the case of classic LECs, this problem might be solved in the future by using well-established methods such as customized (pulsed) electrical stimulation, frozen junctions, and so on. However, more work has to be done in the future to better understand the interactions of QDs and nanocrystals in the LEC environment, as well as to optimize and improve the stability and performance of innovative hybrid devices.

Acknowledgments

My time at Yangzhou University as an undergraduate has come to an end. It's been a voyage of "highs, lows, and averages." We've learnt a lot in the previous four years, and there's still a lot more to learn. I am grateful to Yangzhou University, my instructors, family, and friends for their support.

Prof. Liu, my supervisor, deserves special thanks for his unwavering faith, encouraging words, helpful advice, and steadfast support throughout my journey. When we needed aid or guidance, Teacher Liu was always there for us. With his strict academic approach, acute scientific research perspective, extensive understanding of education, and careful professional devotion, Teacher Liu has always affected me. Teacher Liu is not just my academic advisor, but also my life mentor; his guidance is invaluable to me. I'd want to thank everyone of my research group's seniors, especially my mentors Feiyu Huang, Nan Zhang, and Yang Wang, for teaching and encouraging me throughout the process. They have provided me with a wealth of professional information as well as scientific research methodologies. They did, however, teach me all of the experimental methods, from calculating and weighing the raw ingredients to preparing and describing the results, which was quite beneficial.

I'd want to express my gratitude to Yangzhou University and the college of physical science and technology for providing me with the opportunity to follow my aspirations. Thank you to all of the professors for everything you've done for me; I'll never forget it. I sincerely appreciate the time you spent educating and assisting me on several courses.

Finally, I would like to sincerely thank my family and friends, your concern and support, is my eternal motivation.

References

1. Pei QB, Yu G, Zhang C, Yang Y, Heeger AJ (1995) Science 269:1086
2. Pei QB, Klavetter FL (1994) In: Patent U (ed)
3. Lee JK, Yoo DS, Handy ES, Rubner MF (1996) Appl Phys Lett 69:1686
4. Parker ST, Slinker JD, Lowry MS, Cox MP, Bernhard S, Malliaras GG (2005) Chem Mater 17:3187
5. Shen Y, Kuddes DD, Naquin CA, Hesterberg TW, Kusmierz C, Holliday BJ, Slinker JD (2013) Appl Phys Lett 102:203305
6. Hill ZB, Rodovsky DB, Leger JM, Bartholomew GP (2008) Chem Commun 48:6594
7. Tang S, Tan W-Y, Zhu X-H, Edman L (2013) Chem Commun 49:4926
8. Subeesh MS, Shanmugasundaram K, Sunesh CD, Nguyen TP, Choe Y (2015) J Phys Chem C 119:23676
9. Nishikitani Y, Takeuchi H, Nishide H, Uchida S, Yazaki S, Nishimura S (2015) J Appl Phys 118:225501
10. Weber MD, Adam M, Tykwinski RR, Costa RD (2015) Adv Funct Mater 25:5066
11. Nishikitani Y, Takizawa D, Nishide H, Uchida S, Nishimura S (2015) J Phys Chem C 119:28701
12. Shanmugasundaram K, Subeesh MS, Sunesh CD, Chitumalla RK, Jang J, Choe Y (2015) Org Electron 24:297
13. Subeesh MS, Shanmugasundaram K, Sunesh CD, Won YS, Choe Y (2015) J Mater Chem C 3:4683
14. Weber MD, Nikolaou V, Wittmann JE, Nikolaou A, Angaridis PA, Charalambidis G, Stangel C, Kahnt A, Coutsolelos AG, Costa RD (2016) Chem Commun 52:1602
15. Pertega´s A, Tordera D, Serrano-Pe´rez JJ, Ortı´ E, Bolink HJ (2013) J Am Chem Soc 135:18008
16. Ho C-C, Chen H-F, Ho Y-C, Liao C-T, Su H-C, Wong K-T (2011) Phys Chem Chem Phys 13:17729
17. Jenatsch S, Wang L, Bulloni M, Ve´ron AC, Ruhstaller B, Altazin S, Nu¨esch F, Hany R (2016) ACS Appl Mater Interfaces 8:6554
18. Norell Bader AJ, Ilkevich AA, Kosilkin IV, Leger JM (2011) Nano Lett 11:461
19. Qian G, Lin Y, Wantz G, Davis AR, Carter KR, Watkins JJ (2014) Adv Funct Mater 24:4484
20. Aygu¨ler MF, Weber MD, Puscher BMD, Medina DD, Docampo P, Costa RD (2015) J Phys Chem C 119:12047
21. Zhang H, Lin H, Liang C, Liu H, Liang J, Zhao Y, Zhang W, Sun M, Xiao W, Li H, Polizzi S, Li D, Zhang F, He Z, Choy WCH (2015) Adv Funct Mater 25:7226
22. Meier SB, Hartmann D, Winnacker A, Sarfert W (2014) J Appl Phys 116:104504
23. Edman L (2005) Electrochim Acta 50:3878
24. Costa RD, Ortı´ E, Bolink HJ, Monti F, Accorsi G, Armaroli N (2012) Angew Chem Int Ed 51:8178
25. Slinker JD, Rivnay J, Moskowitz JS, Parker JB, Bernhard S, Abruna HD, Malliaras GG (2007) J Mater Chem 17:2976
26. Sandstro¨m A, Edman L (2015) Energy Technol 3:329
27. Hu T, He L, Duan L, Qiu Y (2012) J Mater Chem 22:4206
28. Leger JM (2008) Adv Mater 20:837
29. Neher D, Gruner J, Cimrova V, Schmidt W, Rulkens R, Lauter U (1998) Polym Adv

Technol 9:461
30. Sun Q, Li Y, Pei Q (2007) J Display Technol 3:211
31. Su H-C, Cheng C-Y (2014) Isr J Chem 54:855
32. Zhang C, Liu ZT, Shen Z, Liu J (2012) Progress Chem 24:1359
33. Inganas O (2010) Chem Soc Rev 39:2633
34. Dini D (2005) Chem Mater 17:1933
35. Q. Pei, A.J. Heeger, Nat. Mater. 7 (2008) 167.
36. G.G. Malliaras, et al. Nat. Mater. 7 (2008) 168.
37. J.C. deMello, Nat. Mater. 6 (2007) 796–797.
38. J.C. deMello, et al. Phys. Rev. B 57 (1998) 12951–12963.
39. J.C. deMello, Phys. Rev. B 66 (2002) 235210.
40. J.C. deMello, et al. Phys. Rev. Lett. 85 (2000) 421–424.
41. J.D. Slinker, et al. Nat. Mater. 6 (2007) 894–899.
42. P. Matyba, et al. Nat. Mater. 8 (2009) 672–676.
43. D.L. Smith, J. Appl. Phys. 81 (1997) 2869–2880.
44. D.J. Dick, et al. Adv. Mater. 8 (1996) 985–987.
45. Y.F. Hu, J. Gao, J. Am. Chem. Soc. 133 (2011) 2227–2231.
46. M. Buda, G. Kalyuzhny, A.J. Bard, J. Am. Chem. Soc. 124 (2002) 6090–6098.
47. H. Rudmann, S. Shimada, M.F. Rubner, J. Appl. Phys. 94 (2003) 115–122.
48. S. van Reenen, et al. J. Am. Chem. Soc. 132 (2010) 13776–13781.
49. A. Munar, et al. Adv. Funct. Mater. 22 (2012) 1511–1517.
50. S. van Reenen, R.A.J. Janssen, M. Kemerink, Adv. Funct. Mater. 22 (2012) 4547– 4556.
51. S. Reineke, K. Walzer, K. Leo, Phys. Rev. B 75 (2007) 125328.
52. M. Lenes, et al. Adv. Funct. Mater. 21 (2011) 1581–1586.
53. M. Lenes, D. Tordera, H.J. Bolink, Org. Electron. 14 (2013) 693–698.
54. S.B. Meier, et al. Phys. Chem. Chem. Phys. 14 (2012) 10886–10890.
55. S.B. Meier, et al. Adv. Funct. Mater. 23 (2013) 3531–3538.
56. T.J. Mills, M.C. Lonergan, Phys Rev B 85 (2012) 035203.
57. S. van Reenen, R.A.J. Janssen, M. Kemerink, Org. Electron. 12 (2011) 1746–1753.
58. H.J. Bolink, et al. Inorg. Chem. 47 (2008) 9149–9151.
59. G.G. Malliaras, J.C. Scott, J. Appl. Phys. 83 (1998) 5399.
60. Z.B. Yu, et al. J. Phys. Chem. Lett. 2 (2011) 367–372.
61. D. Tordera, et al. Adv. Energy Mater. 3 (2013) 1338–1343.
62. C. Murawski, K. Leo, M.C. Gather, Adv. Mater. 25 (2013) 6801–6827.
63. S. van Reenen, et al. J. Am. Chem. Soc. 135 (2012) 886–891.
64. P. Reiss, M. Carrière, C. Lincheneau, L. Vaure, S. Tamang, Chem. Rev. 116, 10731 (2016)
65. J. Park, J. Joo, S.G. Kwon, Y. Jang, T. Hyeon, Angew. Chem. Int. Ed. 46, 4630 (2007)
66. T. Pellegrino, S. Kudera, T. Liedl, A. Muñoz Javier, L. Manna, W.J. Parak, Small. 1, 48(2005)
67. Y. Shirasaki, G.J. Supran, M.G. Bawendi, V. Bulovic, Nat Photon. 7, 13 (2013)
68. F. Todescato, I. Fortunati, A. Minotto, R. Signorini, J. Jasieniak, R. Bozio, Materials 9, 672
(2016)
69. M. Bruchez, M. Moronne, P. Gin, S. Weiss, A.P. Alivisatos, Science 281, 2013 (1998)
70. A.P. Alivisatos, J. Phys. Chem. 100, 13226 (1996)

71. C.D.M. Donega, Chem. Soc. Rev. 40, 1512 (2011)
72. V.I. Klimov, Semiconductor and Metal Nanocrystals: Synthesis and Electronic and Optical Properties (CRC Press, Boca Raton, 2003)
73. P. Reiss, M. Protière, L. Li, Small 5, 154 (2009)
74. M.A. Hines, P. Guyot-Sionnest, J. Phys. Chem. 100, 468 (1996)
75. B.O. Dabbousi, J. Rodriguez-Viejo, F.V. Mikulec, J.R. Heine, H. Mattoussi, R. Ober, K.F. Jensen, M.G. Bawendi, J. Phys. Chem. B. 101, 9463 (1997)
76. X. Peng, L. Manna, W. Yang, J. Wickham, E. Scher, A. Kadavanich, A.P. Alivisatos, Nature 404, 59 (2000)
77. M. Kazes, D.Y. Lewis, Y. Ebenstein, T. Mokari, U. Banin, Adv. Mater. 14, 317 (2002)
78. K.D. Sattler, Handbook of Nanophysics: Nanoparticles and Quantum Dots (CRC Press, Boca Raton, 2016)
79. T. Mokari, U. Banin, Chem. Mater. 15, 3955 (2003)
80. X. Peng, M.C. Schlamp, A.V. Kadavanich, A.P. Alivisatos, J. Am. Chem. Soc. 119, 7019(1997)
81. J.J. Li, Y.A. Wang, W. Guo, J.C. Keay, T.D. Mishima, M.B. Johnson, X. Peng, J. Am. Chem.Soc. 125, 12567 (2003)
82. Y. Chen, J. Vela, H. Htoon, J.L. Casson, D.J. Werder, D.A. Bussian, V.I. Klimov, J.A. Hollingsworth, J. Am. Chem. Soc. 130, 5026 (2008)
83. NREL. Accessed November 2016
84. P.P. Boix, S. Agarwala, T.M. Koh, N. Mathews, S.G. Mhaisalkar, J. Phys. Chem. Lett. (2015)
85. H.J. Snaith, J. Phys. Chem. Lett. 4, 3623 (2013)
86. D.T. Moore, H. Sai, K.W. Tan, D.-M. Smilgies, W. Zhang, H.J. Snaith, U. Wiesner, L.A. Estroff, J. Am. Chem. Soc. 137, 2350 (2015)
87. Y.-Y. Sun, M.L. Agiorgousis, P. Zhang, S. Zhang, Nano Lett. 15, 581 (2015)
88. S. De Wolf, J. Holovsky, S.-J. Moon, P. Löper, B. Niesen, M. Ledinsky, F.-J. Haug, J.-H. Yum, C. Ballif, J. Phys. Chem. Lett. 5, 1035 (2014)
89. J.S. Manser, P.V. Kamat, Nat Photon. 8, 737 (2014)
90. S. Colella, M. Mazzeo, A. Rizzo, G. Gigli, A. Listorti, J. Phys. Chem. Lett. 7, 4322 (2016)
91. D.B. Mitzi, J. Chem. Soc. Dalton Trans. 1 (2001)
92. D.B. Mitzi, Chem. Mater. 13, 3283 (2001)
93. L.C. Schmidt, A. Pertegas, S. Gonzalez-Carrero, O. Malinkiewicz, S. Agouram, G. Minguez Espallargas, H.J. Bolink, R.E. Galian, J. Perez-Prieto, J. Am. Chem. Soc. 136, 850 (2014)
94. Z.-K. Tan, R.S. Moghaddam, M.L. Lai, P. Docampo, R. Higler, F. Deschler, M. Price, A. Sadhanala, L.M. Pazos, D. Credgington, F. Hanusch, T. Bein, H.J. Snaith, R.H. Friend, Nat Nano. 9, 687 (2014)
95. S.A. Veldhuis, P.P. Boix, N. Yantara, M. Li, T.C. Sum, N. Mathews, S.G. Mhaisalkar, Adv. Mater. 28, 6804 (2016)
96. D. Amgar, S. Aharon, L. Etgar, Adv. Funct. Mater. 26, 8576 (2016)
97. A. Pan, B. He, X. Fan, Z. Liu, J.J. Urban, A.P. Alivisatos, L. He, Y. Liu, ACS Nano 10, 7943 (2016)
98. P. Ramasamy, D.-H. Lim, B. Kim, S.-H. Lee, M.-S. Lee, J.-S. Lee, Chem. Commun. 52, 2067(2016)
99. D.D. Athayde, D.F. Souza, A.M.A. Silva, D. Vasconcelos, E.H.M. Nunes, J.C.D. da Costa,

W.L. Vasconcelos, Ceram. Int. 42, 6555 (2016)
100. V. Zardetto, T.M. Brown, A. Reale, A. Di Carlo, J. Polym. Sci. Part B Polym. Phys. 49, 638(2011)
101. M.I. Saidaminov, A.L. Abdelhady, B. Murali, E. Alarousu, V.M. Burlakov, W. Peng, I.Dursun, L. Wang, Y. He, G. Maculan, A. Goriely, T. Wu, O.F. Mohammed, O.M. Bakr, Nat. Commun. 6, 7586 (2015)
102. F. Zhang, H. Zhong, C. Chen, X.-G. Wu, X. Hu, H. Huang, J. Han, B. Zou, Y. Dong, ACS Nano 9, 4533 (2015)
103. P. Tyagi, S.M. Arveson, W.A. Tisdale, J. Phys. Chem. Lett. 6, 1911 (2015)
104. A.B. Wong, M. Lai, S.W. Eaton, Y. Yu, E. Lin, L. Dou, A. Fu, P. Yang, Nano Lett. 15, 5519(2015)
105. J.A. Sichert, Y. Tong, N. Mutz, M. Vollmer, S. Fischer, K.Z. Milowska, R. García Cortadella, B. Nickel, C. Cardenas-Daw, J.K. Stolarczyk, A.S. Urban, J. Feldmann, Nano Lett. 15, 6521 (2015)
106. L. Protesescu, S. Yakunin, M.I. Bodnarchuk, F. Krieg, R. Caputo, C.H. Hendon, R.X. Yang, A. Walsh, M.V. Kovalenko, Nano Lett. (2015)
107. G. Nedelcu, L. Protesescu, S. Yakunin, M.I. Bodnarchuk, M.J. Grotevent, M.V. Kovalenko, Nano Lett. 15, 5635 (2015)
108. A. Swarnkar, R. Chulliyil, V.K. Ravi, M. Irfanullah, A. Chowdhury, A. Nag, Angew. Chem.Int. Ed. 54, 15424 (2015)
109. H. Huang, F. Zhao, L. Liu, F. Zhang, X.-G. Wu, L. Shi, B. Zou, Q. Pei, H. Zhong, A.C.S. Appl, Mater. Interfaces 7, 28128 (2015)
110. S. Zhuo, J. Zhang, Y. Shi, Y. Huang, B. Zhang, Angew. Chem. 127, 5785 (2015)
111. H. Zhu, Y. Fu, F. Meng, X. Wu, Z. Gong, Q. Ding, M.V. Gustafsson, M.T. Trinh, S. Jin, X.Y. Zhu, Nat. Mater. 14, 636 (2015)
112. H. Huang, A.S. Susha, S.V. Kershaw, T.F. Hung, A.L. Rogach, Adv. Sci. 2, 1500194 (2015)
113. S. Gonzalez-Carrero, R.E. Galian, J. Perez-Prieto, J. Mater. Chem. A. 3, 9187 (2015)
114. O. Vybornyi, S. Yakunin, M.V. Kovalenko, Nanoscale 8, 6278 (2016)
115. Q.A. Akkerman, V. D'Innocenzo, S. Accornero, A. Scarpellini, A. Petrozza, M. Prato, L. Manna, J. Am. Chem. Soc. 137, 10276 (2015)
116. Y. Tong, E. Bladt, M.F. Aygüler, A. Manzi, K.Z. Milowska, V.A. Hintermayr, P. Docampo, S. Bals, A.S. Urban, L. Polavarapu, J. Feldmann, Angew. Chem. Int. Ed. 55, 13887 (2016)
117. Y. Bekenstein, B.A. Koscher, S.W. Eaton, P. Yang, A.P. Alivisatos, J. Am. Chem. Soc. 137,16008 (2015)
118. D. Zhang, S.W. Eaton, Y. Yu, L. Dou, P. Yang, J. Am. Chem. Soc. 137, 9230 (2015)
119. A.J.N. Bader, A.A. Ilkevich, I.V. Kosilkin, J.M. Leger, Nano Lett. 11, 461 (2011)
120. G. Qian, Y. Lin, G. Wantz, A.R. Davis, K.R. Carter, J.J. Watkins, Adv. Funct. Mater. 24,4484 (2014)
121. J. Frohleiks, S. Wepfer, Y. Kelestemur, H.V. Demir, G. Bacher, E. Nannen, A.C.S. Appl, Mater. Interfaces. 8, 24692 (2016)
122. S. Coe, W.-K. Woo, M. Bawendi, V. Bulovic, Nature 420, 800 (2002)
123. M.F. Aygüler, M.D. Weber, B.M.D. Puscher, D.D. Medina, P. Docampo, R.D. Costa, J. Phys. Chem. C 119, 12047 (2015)
124. B.M.D. Puscher, M.F. Aygüler, P. Docampo, R.D. Costa, Adv. Energy Mater.

125. H. Zhang, H. Lin, C. Liang, H. Liu, J. Liang, Y. Zhao, W. Zhang, M. Sun, W. Xiao, H. Li, S. Polizzi, D. Li, F. Zhang, Z. He, W.C.H. Choy, Adv. Funct. Mater. 25, 7226 (2015)
126. A.J. Nozik, Phy. E 14, 115 (2002)